Polymer-Filled Nanoporous Membranes

A Thesis

Submitted to the Faculty

of

Drexel University

by

Sunil Raghav

in partial fulfillment of the

requirements for the degree

of

Master of Science in Chemical Engineering

June 2005

`

Dedications

This thesis is dedicated to my parents Lt. Col. Gobind Ram Raghav and Suresh Raghav, and sisters Shalini Verma and Vandana Raghav for their unconditional love and support throughout my life.

Acknowledgements

I would like to thank the following individuals for their help in the completion of this project:

My committee members Dr. Nily Dan and Dr. Giuseppe Palmese, for taking time to review my thesis and serving on my committee.

A special thanks goes to my advisor, Dr. Yossef A. Elabd who spent considerable time in planning experiments and analyzing my data.

And finally, thanks to Puja who has helped me in innumerable ways throughout this project. Thank you for your relentless love and support, with you by my side I will accomplish great things.

TABLE OF CONTENTS

LIST OF TABLES

LIST OF FIGURES

ABSTRACT
Polymer-Filled Nanoporous Membranes
Sunil Raghav
Yossef A. Elabd, Ph.D.

Recent studies in our laboratory have demonstrated the effect of nanostructure on proton conductivity. In this study, oriented nanostructured polymer membranes were fabricated by conjoining an ion conductive polymer with nanoporous host membranes, which have uniform pores aligned normal to the plane of the membrane. The hypothesis of research is that by orienting the ionic nanostructure of an ion conductive polymer, the ion transport will therefore increase. A number of strategies were employed to maximize pore-filling efficiency and control the thickness of the resulting composite membrane. For example, track-etched polycarbonate and porous alumina membranes (both of which have straight and cylindrical pores aligned normal to the plane of the membrane) were filled with sulfonated polystyrene using various physical sorption techniques at a variety of pore sizes. The structures of these membranes were characterized using SEM, and the proton conductivity was studied using electrochemical impedance spectroscopy. Transport structure-property relationships were analyzed based on these results.

CHAPTER 1: INTRODUCTION

1.1 Polymer electrolyte membranes (PEMs)

Phase segregation occurs in proton conducting polymers during solvent casting [1]. Aggregation of ions occurs as a result of electrostatic interactions between ion pairs, leading to the formation of two phases: an *ion-rich phase (i.e.* ion clusters*)* and an *ion-poor phase*. Figure 1.1 shows the concept of microphase separation in a PEM. The polymer separates into regions of ion clusters and nonionic clusters. It is believed that protons migrate from one ionic cluster to the other through water channels that connect ionic clusters. Gierke et al. [5] determined the ionic nanostructure of Nafion® by X-ray analysis and suggested ion clusters approximately 5 nm in size interconnected by small narrow ionic channels on the order of 1 nm .

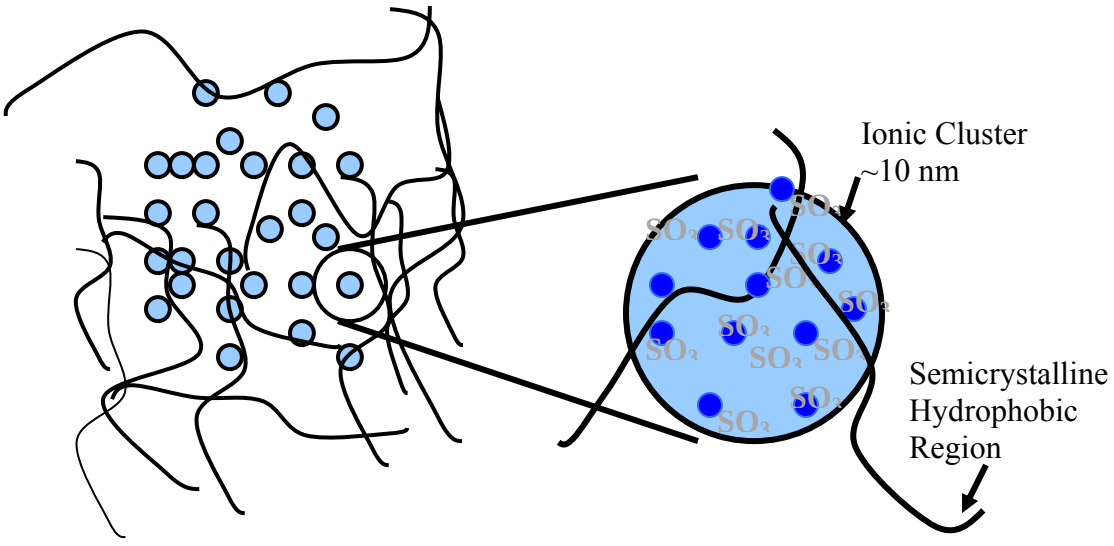

Figure1.1 Schematic of microphase separation in a hydrated ionomer.

There are two different transport mechanisms for protons in PEMs. The first is the *Grotthuss mechanism*, where the proton hop from one ion rich site to the other [2]. The second is e*lectroosmotic drag,* where protons diffuse through the membrane, attached to water as hydronium ions, H_3O^+ [3]. Proton transport is also dependent on polymer morphology or ionic nanostructure [4]. A few examples of PEMs include Nafion®, sulfonated polystyrene, sulfonated poly[bis(3-methylphenoxy)]phosphazene and sulfonated poly (ether ketone).

1.2 Applications of PEMs

PEMs have been used in a variety of electrochemical applications, such as actuators, sensors, electrolysis, and low-temperature fuel cells. The principle operation in each of these applications remains the same: the ability of the ions to conduct across the membrane. To date, researchers have developed a variety of new membranes for fuel cells. Examples of strategies include: sulfonation of homopolymers [6], block copolymers [7], doping polymers with acids [8], grafting sulfonic acid side chains onto polymers [9], sol-gel chemistry to produce hybrids with heteropolyacids [10], embedding zeolites into polymers [11] and various composites of Nafion® (the most common PEM used in fuel cells).

Researchers have used PEMs for applications in actuation [12, 13]. The most important and oldest industrial application is the electrolysis of sodium/calcium chloride solutions [14]. The PEM is used as a separator between the half cells.

Nafion® membranes were used recently in sensors at room temperature [15, 16, 17], where oxygen determination of these sensors were either potentiometric or amperometric. Nafion® membranes work well as proton conductors at room temperature and are therefore more economical. Kuwata et al. [15] used an amperometric sensor for oxygen determination consisting of an electrochemical cell combined with a hydrogen-generation system and a gas diffusion layer. The sensing current under the short circuit condition was found to vary linearly with the partial pressure of the oxygen. Morris et al. [16] developed sensors of potentiometric type for hydrogen, oxygen and water using Nafion® membranes. Sima et al. [17] developed a simple oxygen sensor with Nafion® membrane as the electrolyte that may be developed in any size or shape. This sensor can provide direct information on oxygen permeation, which is the main reason for the deterioration of paint films. Smela et al. [31] described the use of oriented conducting polymers in synthesis of actuators.

1.3 Anisotropy in PEMS

Ionic block copolymers have a highly ordered sequence of repeating ionic and non-ionic blocks (unlike random copolymers which have no definite repeating pattern for ionic and non-ionic blocks). Researchers have observed that ionic block copolymers self assemble into oriented nanostructured morphologies [18, 19, 20]. In particular, Elabd et al. [20] measured the conductivities of an ionic block copolymer and observed anisotropic conductivities. Cable et al. [21] stretched Nafion® and induced an ionic orientation in

plane of the membrane. The proton conductivity was higher in plane of the membrane than normal to plane of the membrane. Recently, Oren et al. [22] found that the conductivities for aligned membranes were higher for anisotropic membranes than that for isotropic membranes. These studies reveal the significant impact that organized and oriented structures can have in increasing proton conductivity. Libby at al. prepared composite membranes by embedding zeolite particles within a polyvinyl alcohol polymer matrix. Although their membrane did not achieve higher proton conductivity as compared to a pure Nafion® membrane, they did succeed in demonstrating (through calculations) that the embedded conducting material could be aligned through a membrane.

1.4 Alignment of ionic channels: polymer filled porous membranes

One approach to aligning ion rich domains normal to the plane of the membranes is to use porous membranes that have pores aligned in that direction (Figure 1.2). A strategy is to use track-etched membranes. Track-etched polymer membranes provides a unique host matrix with straight pores oriented normal to the plane with a controlled pore size on the order of 10 nm. Researchers have already found use of track-etched membranes in the synthesis of nanowires and nanotubes [23, 24, 25, 26]. The general strategy employed by these researchers was to fill the pores of these membranes with polymers or metals and then use a solvent to dissolve the track-etched membrane, leaving behind nanowires.

On the electrochemical aspect of using such host membranes, Fang at al. [27] examined the flux of cations in track-etched polycarbonate (PCTE) filled with Nafion® using steady-state rotation disk voltammetry. They observed that as the diameter of the

nanopores decreased, the cation flux increased by as much as 20-fold compared to solution-cast Nafion® films. This study demonstrated that confinement of a polymer within the pores of a track-etched membrane leads to an increase in transport. Vorrey et al. [28] studied the effects of filling track-etched PC with polyethylene oxide (PEO) on electrical conductivity. Conductivity increased by two orders of magnitude by decreasing pore size from 400 to 30 nm.

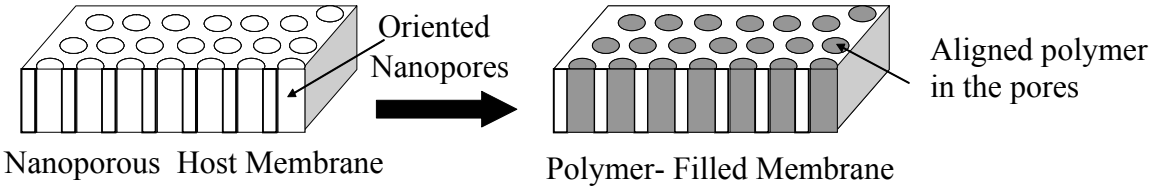

Figure 1.2 Schematic showing the strategy for aligning polymer electrolyte in the pores of a host membrane.

Yamaguchi et al. [29, 30] filled the pores of high density polyethylene with poly(acrylamide-tert-butyl sulfonic acid) and observed high proton conductivities and low swelling for the polymer confined in the pores.

1.5 Drawbacks of past research on polymer filled porous membranes

One drawback of past research is that polymer-filled porous membranes have not been characterized with SEM. Fang et al. [27] claim that Nafion® (5 g/100 mL) in a solution of water/alcohol completely fills the pores of track-etched membranes by sorption alone.

These results could not be reproduced in our laboratory. Figure 1.3 shows that Nafion® does not sorb into the pores of PCTE membranes.

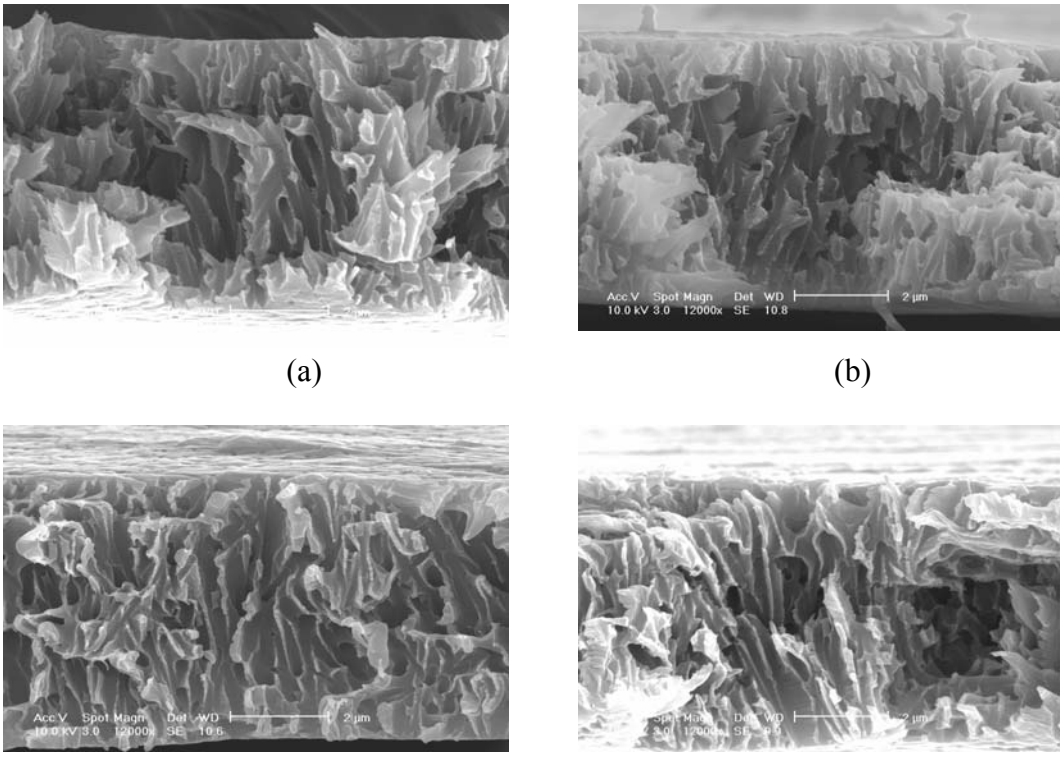

Figure 1.3 SEM images of the cross-section of PCTE membranes after being sorbed in Nafion® solution.

In this research project, the structures of the fabricated membranes have been characterized with SEM and the transport properties have been analyzed with respect to the structure of the fabricated membrane. The transport properties have been analyzed as a function of the pore size, pore density and thickness of the fabricated membrane.

CHAPTER 2: EXPERIMENTAL

2.1 Material

2.1.1 Porous host membranes

Polycarbonate track-etched (PCTE) membranes of 100 nm, 50 nm and 10 nm pore diameters purchased from GE Osmonics and porous alumina of 100 nm and 20 nm pore diameters purchased from Whatman were used as host membranes (Figure 2.1). PCTE membranes have discrete pores that are formed through a combination of charged-particle bombardment (or irradiation) and chemical etching. This particle bombardment results in the formation of damaged areas in the film (or tracks), which are subsequently etched to form discrete pores with a defined pore size. The track-etched membranes have a porosity of approximately 1 % and are 6 microns in thickness. Porous alumina membranes are composed of a high purity alumina matrix that is manufactured electrochemically. They contain a densely packed array of regular, near hexagonal shaped pores. The structure is non-deformable and there are no lateral crossovers between the pores. The porous alumina membranes are made via anodization of aluminum metal foils in an acidic solution. The alumina membranes are typically 50 % in porosity and are 58 microns thick. The surface and cross-sectional views of these membranes showing the pores were characterized by scanning electron microscopy (SEM) and are shown in Figure 2.1.

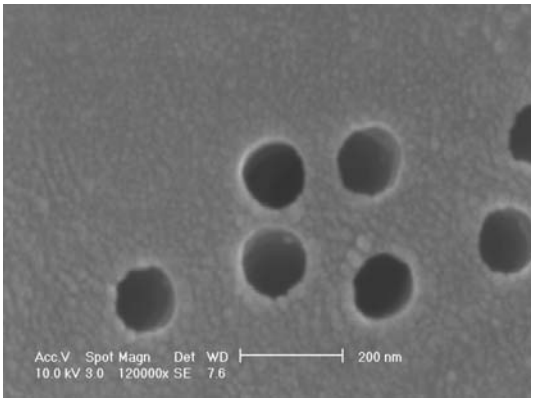

(a)

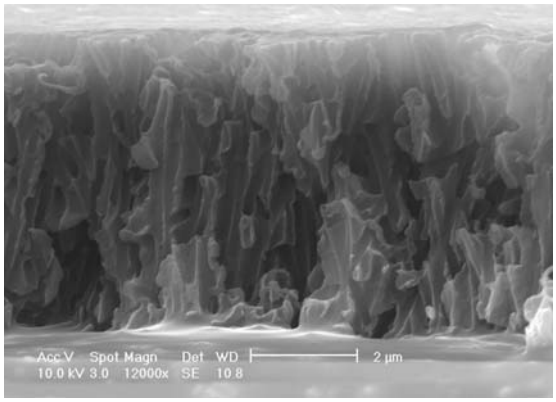

(b)

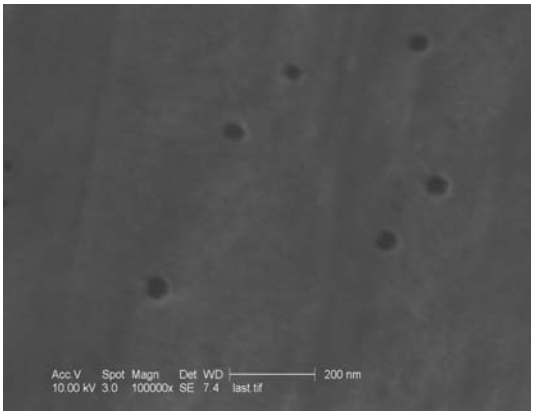

(c)

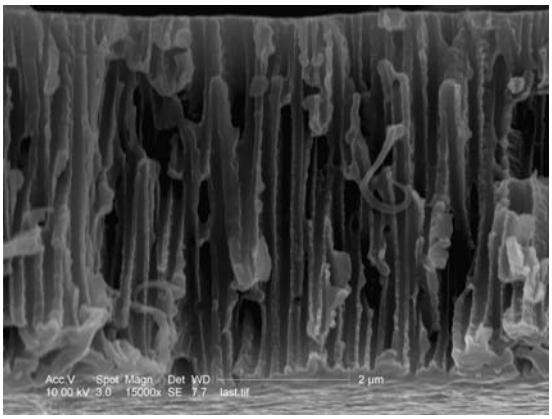

(d)

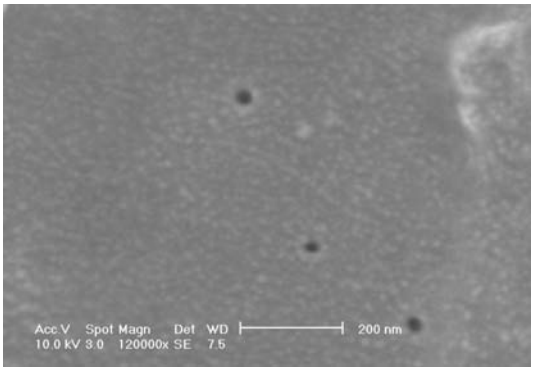

(e)

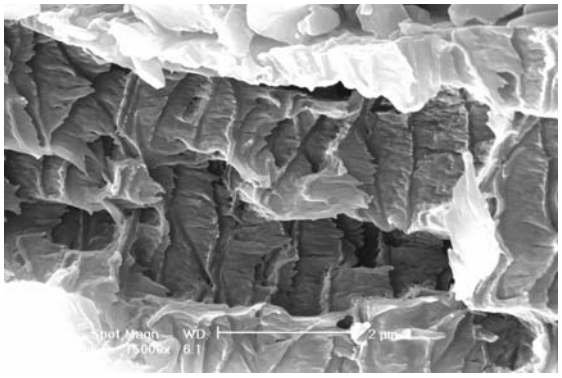

(f)

Figure 2.1 SEM images of the porous host membranes (a) 100 nm PCTE, top view (b) 100 nm PCTE, cross-sectional view (c) 50 nm PCTE, top view (d) 50 nm PCTE, cross-sectional view (e) 10 nm PCTE, top view (f) 10 nm PCTE, cross-sectional view (g) 20 nm alumina, top view (h) 20 nm alumina, cross-sectional view (i) 100 nm alumina, top view (j) 100 nm alumina, cross-sectional view.

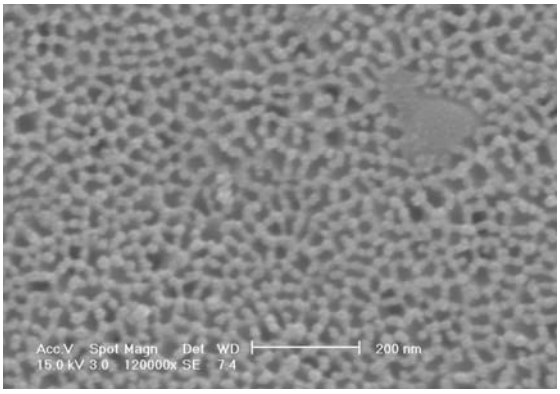

(g)

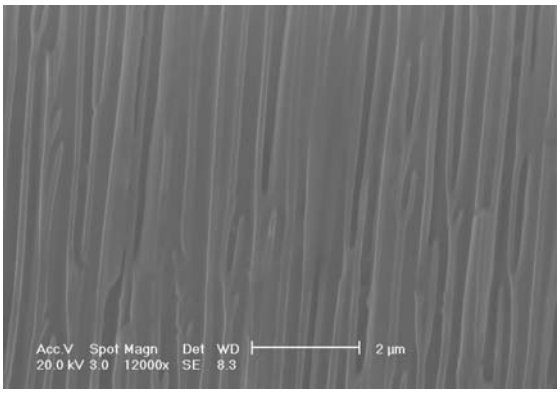

(h)

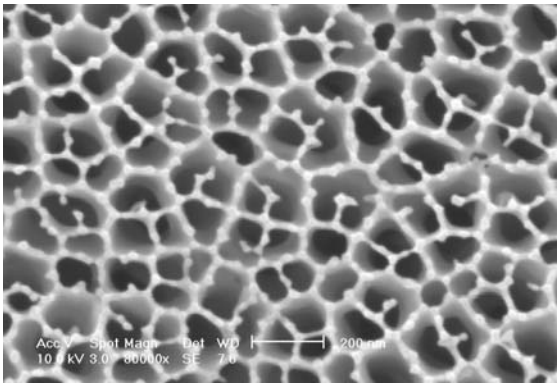

(i)

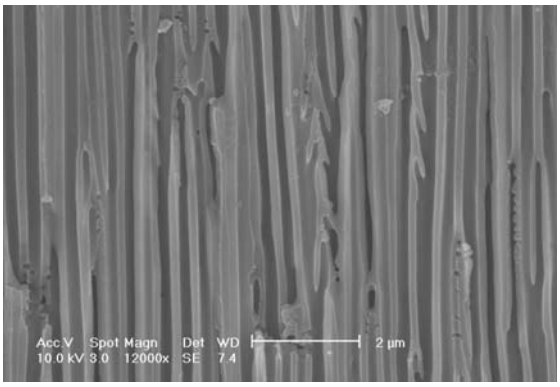

(j)

Figure 2.1 (*continued)*

The porous host membranes have been specified according to the pore size, porosity and thickness. This data is presented in Table 2.1.

Table 2.1 Porous membrane specifications.

Membrane Type	Pore size (nm)	Porosity (%)	Nominal Thickness (μm)	Manufacturer
Track-Etched Polycarbonate	10, 50, 100	1	6	GE Osmonics
Porous Alumina	20, 100	50	58	Whatman

2.1.2 Polymer electrolyte

Sulfonated polystyrene (SPS) was used as the conductive filling polymer. Polystyrene was sulfonated according to the procedure described below. Polystyrene was determined to be 43 mol % sulfonated by titration and elemental analysis. Acetone and dimethyl sulfoxide (DMSO) were used as solvents for SPS. Nafion® purchased from Ion Power and Aldrich has also been used as the polymer electrolyte.

2.1.2.1 Sulfonation of polystyrene

50 g polystyrene (PS) and 500 ml dichloromethane (DCM) (10% w/v) were mixed in a 1 L three-neck flask. The flask was covered with aluminum foil and the contents were stirred continuously. The flask was heated at 40^{o}C under reflux conditions. In a 500 mL flask, 200 mL of DCM was chilled. 60 mL of acetic anhydride was added to the chilled DCM. 26 mL of sulfuric acid was added to DCM. After 10 minutes, the sulfuric acid/DCM mixture was removed from the ice bath and allowed to equilibrate (with stirring) at room temperature. Once 40 ^{o}C had been attained in the three-neck flask, the

sulfuric acid/DCM mixture was slowly poured into the three-neck flask. The reaction was allowed to proceed for 4 hours and was terminated by adding 300 mL of methanol.

The above polymer solution was washed with deionized water to remove acid and filtered to remove water. This step was repeated until the pH reached 2-3 and was stirred with water overnight. The polymer was redissolved in methanol and heated in a convection oven at 50^{o}C. The polymer was washed with water. The redissolving/drying/washing step was repeated to remove residual acid. pH was monitored after each step until the mixture became neutral.

Titration was performed by dissolving 0.1g SPS in approximately 40 mL of methanol in a small beaker. The mixture was stirred until SPS dissolved completely. NaOH (0.01239 M in methanol) was added to a burette. The base level of NaOH was recorded. 10-15 drops of thymol blue (0.1 % w/v in methanol) indicator were mixed into the SPS/methanol mixture. The SPS/methanol/thymol blue mixture was kept stirring while NaOH was added dropwise. At a certain point, the mixture turned pale yellow. This point marked the end point and the volume of NaOH consumed was recorded. Eight titrations were performed. Table 2.2 lists the titration results.

The percentage sulfonation was calculated as:

$$\%sulfonation = \frac{(mol_{SO_3})}{(mol_{PS})}$$

The moles of SO_3 were calculated as:

$mol_{SO3} = moles\ of\ NaOH\ \ used$

The moles of PS were calculated as:

$$mol_{PS} = \frac{(wt of\ SPS) - (mol_{SO_3})(MW_{SO_3})}{MW_{PS}}$$

Table 2.2 Titration results for sulfonated polystyrene.

Titration No.	Amount of NaOH added (mL)	Weight of SPS (g)	Sulfonation mol %
1	26.0	.1011	49.19
2	25.0	.0986	43.63
3	24.8	.0984	43.29
4	25.2	.1003	43.11
5	25.1	.0972	44.72
6	25.6	.0974	45.92
7	27.9	.1168	40.14
8	26.9	.1012	46.50

The average sulfonation level as calculated from the above table was 44.56 mol %. Elemental analysis was performed on the sulfonated polymer at Atlantic Microlab Inc. and the sulfonation level was determined to be 43.48 mol %. The average value of the level of sulfonation as determined by titration was in close agreement with that determined by elemental analysis.

2.2 Equipment

The proton conductivity of each polymer membrane was determined by AC impedance spectroscopy. The measurements were taken between 100 Hz and 1 MHz using a Solartron AC impedance system (1260 impedance analyzer, 1287 electrochemical interface, Zplot software). The prehydrated membrane was quickly put in a two – electrode conductivity cell (Figure 2.2) and sealed off. Tests were performed at room temperature and saturation. The Z-Plot software varies the current frequeny and plots the imaginary vs. the real impedance. The membrane resistances were calculated from the x-intercept of a linear regression of the data from 10^6 to 10^4 Hz . A digital micrometer (Mitutoyo) was used to measure the membrane thickness. The conductivities were calculated using the formula:

$$\kappa = L/AR$$

where κ is the conductivity (S/cm), L is the thickness of the membrane (cm), A is the electrode cross-sectional area (1.22 cm^2) and R is the membrane resistance (Ω). The cell shown in Figure 2.2 is referred to as a two-electrode cell and is comprised of two stainless steel blocking electrodes that sandwich the membrane. A Teflon® casing provides support to the electrodes and prevents membrane dehydration. This conductivity cell was manufactured at the Hess Laboratory Machine shop (Drexel University).

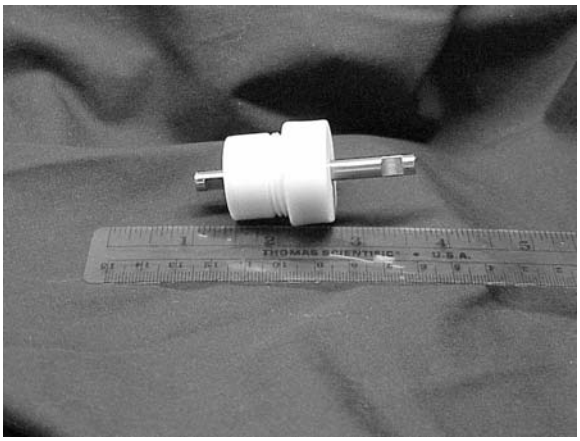

Figure 2.2 Two-electrode conductivity cell.

Spincoating (Figure 2.3) was used to control the thickness of the polymer layer on top of the porous host membrane. This was done to study conductivity as a function of composite thickness. The spincoater used was manufactured by Speciality Coating System (Model P-6708). Vacuum was applied to hold the silicon wafer disk onto the spinning chuck (Figure 2.4). The silicon disk held the porous host membrane on top, where a layer of the conducting polymer was present (still in a wet form). The chuck was rotated at different speeds and different times. The spuncoat membranes were then dried in a vacuum oven at 100^{o}C for one day.

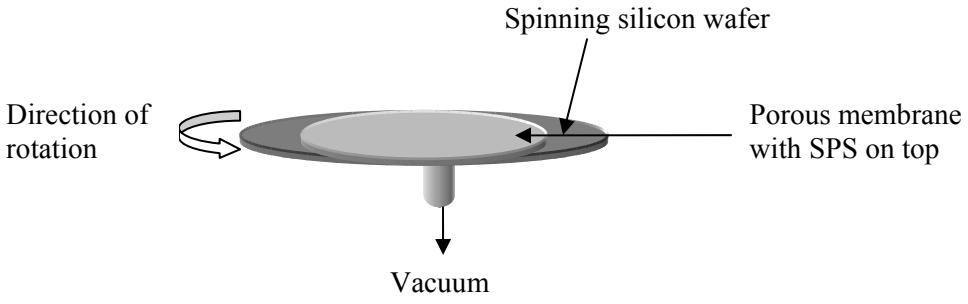

Figure 2.3 Schematic representation of the spincoating process.

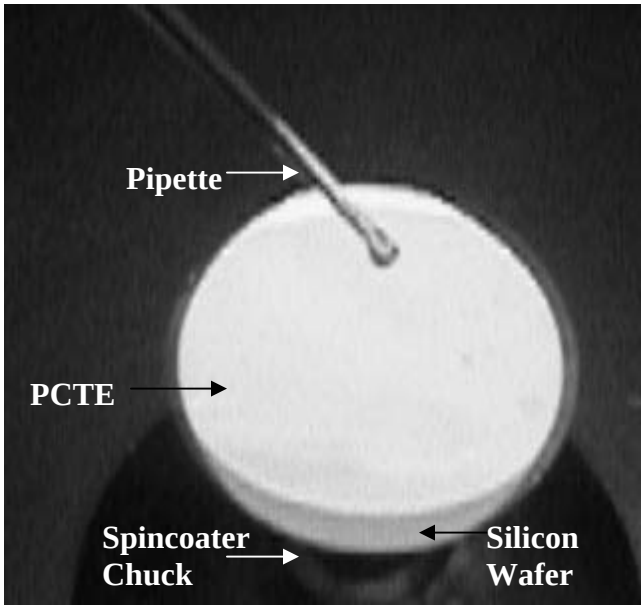

Figure 2.4 The spincoating setup.

Figure 2.5 The field emission environmental scanning electron microscope (ESEM)

The membranes were fractured, sputtered with gold-palladium or platinum in a sputter machine (Figure 2.6) for 40 seconds, and then observed under a field fmission fnvironmental scanning electron microscope (SEM), model FEI/Phillips XL30 (Figure 2.5).

Figure 2.6 Denton II sputter coater.

The viscometer used was a Brookfield HBTD digital viscometer (Figure 2.7), which has a spindle number range of 40 to 1.6M cP and 10 speeds from 0.5 to 100 RPM. The unit measures viscosity by sensing the torque needed to rotate a spindle at a constant speed in 600 ml or more of test fluid. Torque is proportional to the viscous drag on the spindle and thus to the viscosity of the fluid. Low, medium and high viscosity measurements are possible with accuracies within 1% of the range in use, and a reproducibility of 0.2%. The apparatus was setup so that the spindel was fully vertical and not touching the walls of the outer cylinder. The fixed volume of the solution was filled in the inner cylinder.

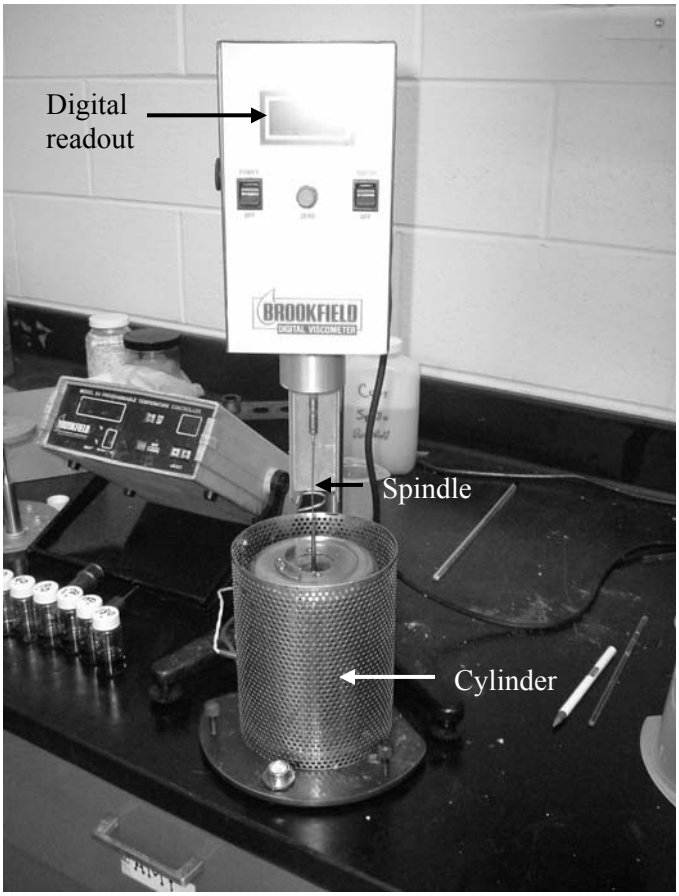

Figure 2.7 Brookfield HBTD digital viscometer.

Maximum speed (RPM) was set at full clockwise rotation and minimum speed at full counter-clockwise rotation. The speed setting is indicated by the number on the knob located opposite the button on the Viscometer housing. At steady states, the reading was noted. All data was collected at 79^{o}F.

One of the important characteristics of a liquid penetrant material is its ability to freely wet the surface of the object being inspected. At the liquid-solid surface interface, if the molecules of the liquid have a stronger attraction to the molecules of the solid surface

than to each other (the adhesive forces are stronger than the cohesive forces), then wetting of the surface occurs. Alternately, if the liquid molecules are more strongly attracted to each other and not the molecules of the solid surface (the cohesive forces are stronger than the adhesive forces), then the liquid beads-up and does not wet the surface.

One way to quantify a liquid's surface wetting characteristics is to measure the contact angle of a drop of liquid placed on the surface of the subject object. The contact angle is the angle formed by the solid/liquid interface and the liquid/vapor interface measured from the side of the liquid (Figure 2.8). Liquids wet surfaces when the contact angle is less than 90 degrees. For a penetrant material to be effective, the contact angle should be as small as possible. In fact, the contact angle for most liquid penetrants is very close to zero degrees.

Wetting ability of a liquid is a function of the surface energies of the solid-gas interface, the liquid-gas interface, and the solid-liquid interface. The surface energy across an interface or the surface tension at the interface is a measure of the energy required to form a unit area of new surface at the interface. The intermolecular bonds or cohesive forces between the molecules of a liquid cause surface tension. When the liquid encounters another substance, there is usually an attraction between the two materials.

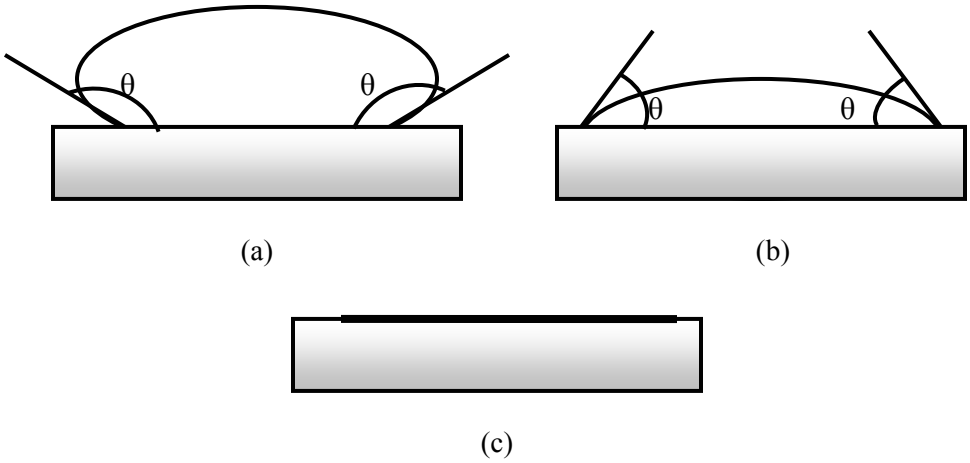

Figure 2.8 Contact angles for (a) repelling, (b) spreading and (c) penetrating fluids.

The adhesive forces between the liquid and the second substance will compete against the cohesive forces of the liquid. Liquids with weak cohesive bonds and a strong attraction to another material (or the desire to create adhesive bonds) will tend to spread over the second material. Liquids with strong cohesive bonds and weaker adhesive forces will tend to bead-up or form a droplet when in contact with the second material.

In liquid penetrant testing, there are usually three surface interfaces involved, the solid-gas interface, the liquid-gas interface, and the solid-liquid interface. For a liquid to spread over the surface of a part, two conditions must be met. First, the surface energy of the solid-gas interface must be greater than the combined surface energies of the liquid-gas and the solid-liquid interfaces. Second, the surface energy of the solid-gas interface must exceed the surface energy of the solid-liquid interface.

For measuring the contact angles of the fluids, the PCTE membrane was taped onto a clean glass slide. The camera was focused onto the membrane, to get good resolution and high magnification. The polymer solution was filled into the 10 mL syringe and the flow rate was controlled. The polymer solution was injected from the 10 mL syringe onto the PCTE membrane at 0.5 mL/hour. The pictures were taken after 3 drops of the solution had been deposited. The steps were performed 3-4 times for each polymer solution. All data was collected at 79^{o}F. The contact angles were measured using a protractor.

CHAPTER 3: PHYSICAL SORPTION METHODS

The experimental procedures include methods to fill the pores of host membranes (sorption and vacuum filtration) and methods to control or reduce the thickness of the composites (spincoating and blotting). The membranes that were fabricated were characterized by AC impedance spectroscopy and SEM.

3.1 Sorption

PCTE or alumina membranes were soaked in a SPS/acetone solution 5 % (w/v) for 24 hours. The excess solution was drained off the surface (by holding the membrane in a tilted position) and the membranes were dried at 100^{o}C under vacuum for 24 hours. The membranes were then cut into circular pieces for conductivity tests. In some cases, the PCTE membranes were sulfonated before membrane preparation. Figure 3.1 shows both PCTE and sulfonated PCTE, where PCTE was sulfonated using a similar procedure as SPS. When the FTIR-ATR spectra of PCTE and sulfonated PCTE were compared, the additional peak at 1005 cm^{-1} confirms the presence of sulfonic acid groups on PCTE. The in-plane bending vibrations of the aromatic ring parasubstituted with the sulfonate group is represented at 1005 cm^{-1}[32].

Control over the thickness of the composites could not be achieved by using the sorption technique as depicted in Figure 3.2. Generally, composites with $L_t/L_b>5$ were synthesized, where L_t is the thickness of the top SPS layer and L_b is the thickness of the

bottom composite layer. It was also observed that the pores of the sorbed membranes were not completely filled with SPS, as depicted in Figure 3.2.

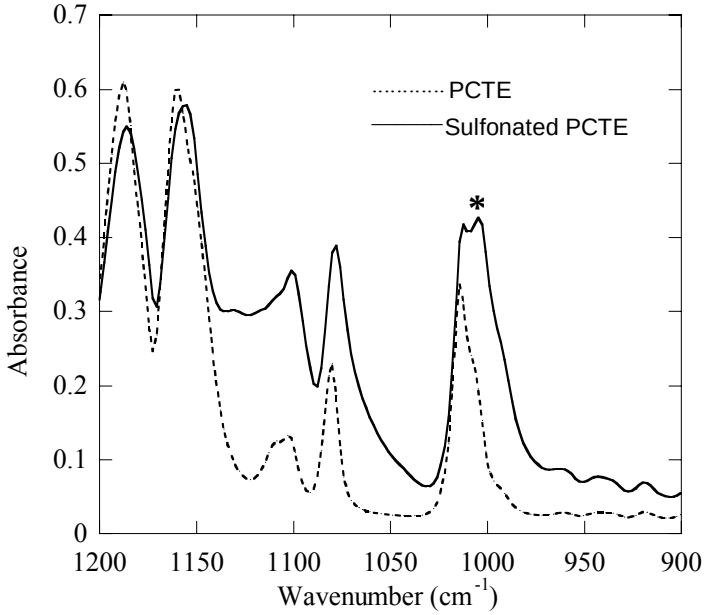

Figure 3.1 The FTIR-ATR spectra of PCTE and Sulfonated PCTE. ***** represents the additional peak due to sulfonation.

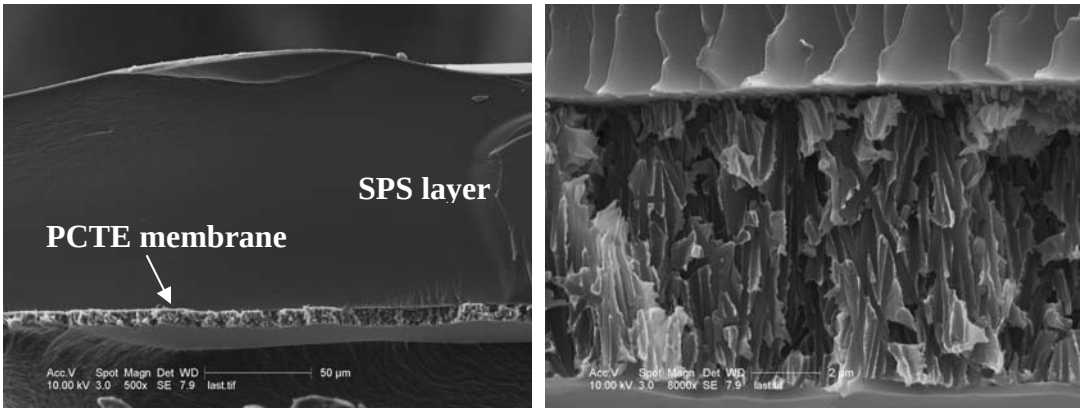

Figure 3.2 SEM of a sorbed SPS/PCTE composite membrane.

For the composites fabricated by sorption, there seemed to be no correlation between structure and conductivity (Figure 3.3).

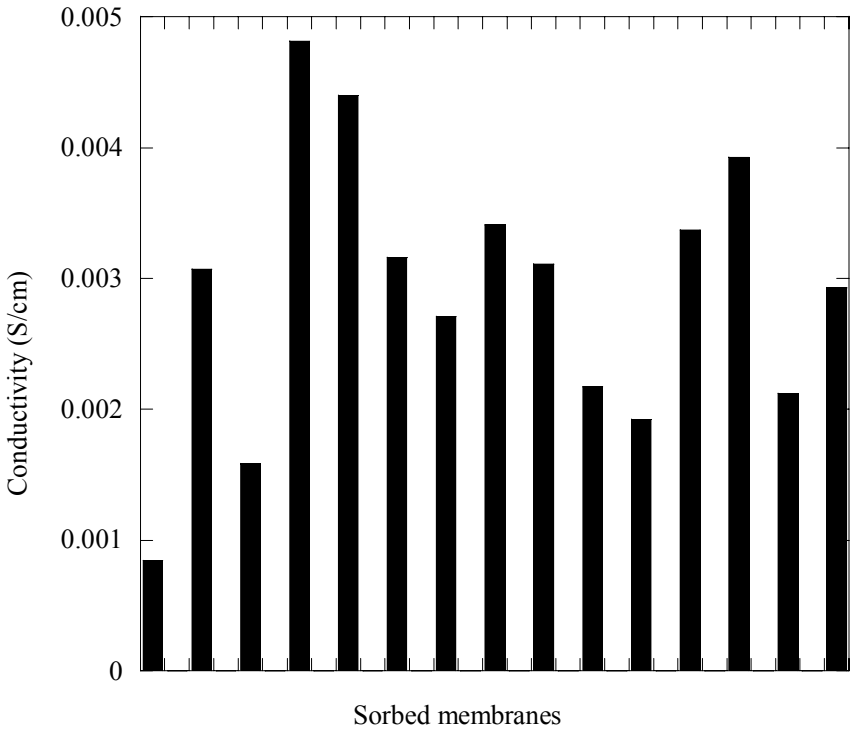

Figure 3.3 Conductivity data for SPS/PCTE composites prepared by sorption.

The data was next studied as a function of the thickness. Figure 3.4 is a plot of the conductivities of the membranes versus L_t/L_b. As can be seen from the plot, the conductivities of the membranes change with the thickness of the membranes.

The conductivities increase with increasing values of L_t/L_b. The value of conductivity is 2.3×10^{-3} S/cm at L_t/L_b =5.66 and increases to 1.7×10^{-2} S/cm for L_t/L_b =15.66. This is

almost an order of magnitude increase in conductivity for a 3-fold increase in the value of L_t/L_b.

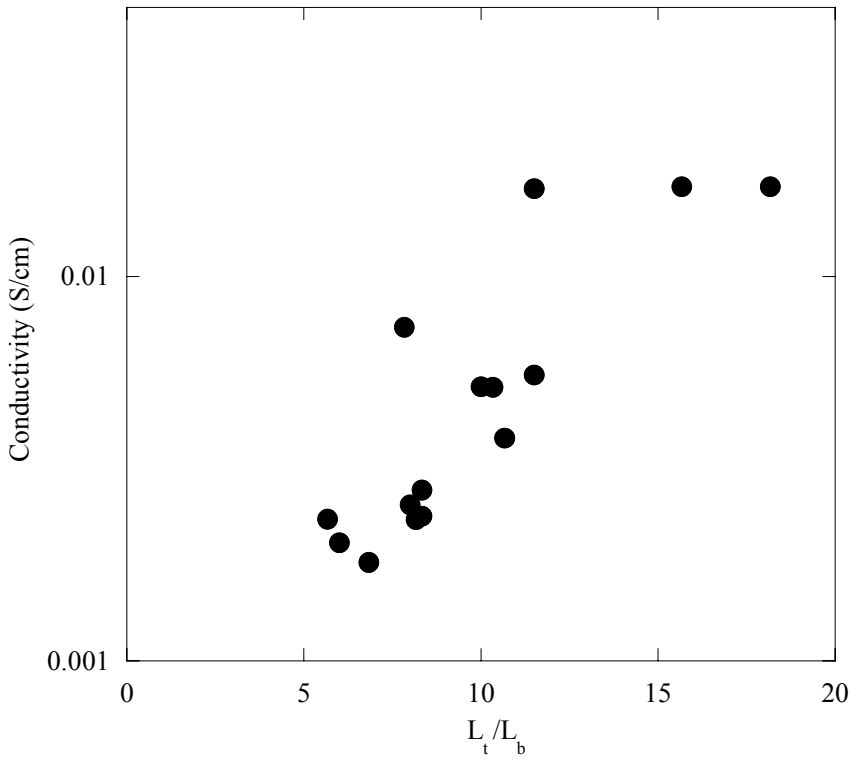

Figure 3.4 Conductivity versus thickness for sorbed PCTE membranes.

3.2 Spincoating

The thickness of the composite membranes can be controlled via spincoating, as shown in Figure 3.5. Figure 3.6 shows that thinner membranes can be achieved at higher spincoating speeds. Also, $L_t/L_b < 1$ is possible at spincoating speeds greater than 500 RPM. The value of L_t/L_b is 1.055 at 500 RPM spincoater speed and decreases to 0.222 as the spincoater speed is increased to 2500 RPM.

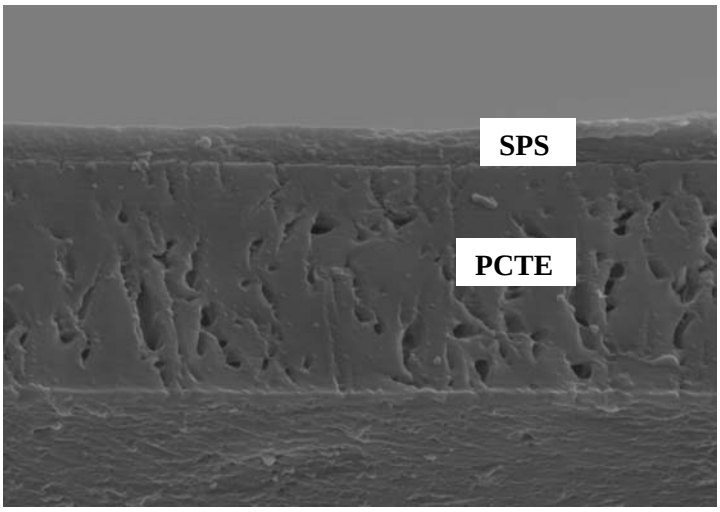

Figure 3.5 SEM of a spuncoat PCTE membrane.

From Figure 3.5, the thickness of the spuncoat membrane is $L_t/L_b<1$. Fifteen membranes were spuncoat as a function of the spincoater speed (three membranes at each speed). There also seems to be higher control over the thickness as spincoater speed increases, as can be seen from the smaller error bars at higher spinning speeds.

Figure 3.6 also confirms that $L_t/L_b<1$ can be achieved through spin coating. An average value of Lt/Lb=0.2 was obtained at 2500 RPM. The average value of L_t/L_b was 1.0556 at 500 RPM.

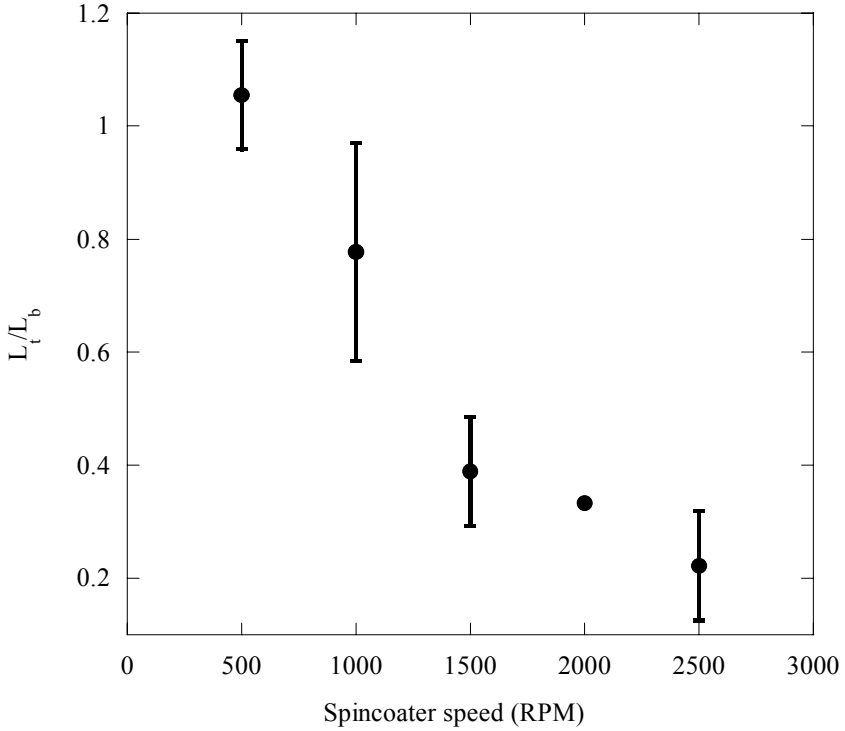

Figure 3.6 Thickness and spincoater speed for composite membranes.

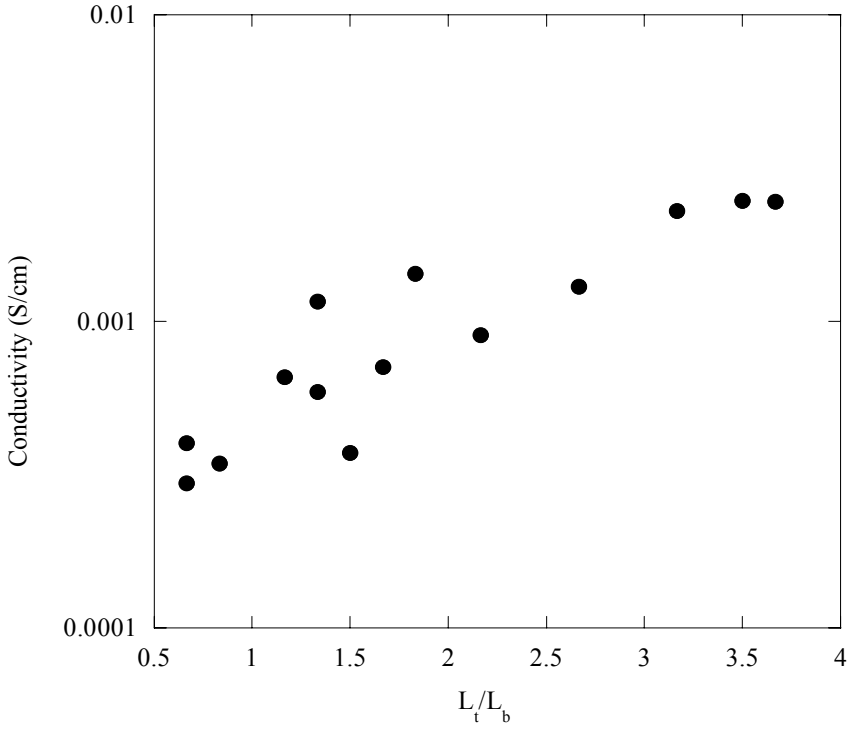

Figure 3.7 Conductivity versus L_t/L_b for spuncoat membranes.

Figure 3.7 shows increasing values of conductivities for increasing thickness of the composites, confirming the relationship between conductivity and thickness. The value of conductivity is 3.43 x 10^{-4} S/cm at a value of L_t/L_b=0.83333 and increased to 2.4708 x 10^{-3} S/cm at a value of L_t/L_b =3.5. This is almost an order of magnitude increase in conductivity for a 4-fold increase in the value of L_t/L_b. A model was developed to explain the conductivity-thickness dependence for the composites, which is described in the next section.

3.3 The conductivity model

It became apparent from the study described earlier that composite membranes displayed different conductivities for the same pore-filling protocol at different thicknesses. As a result, it became necessary to include the thickness of the SPS layer as a parameter that affected conductivity. Therefore, a model was developed to explain these results.

A series resistance model was used, in which the protons diffusing across the composite membrane face two kinds of resistances, the first due to the SPS layer and the second due to the PCTE membrane. The overall resistance faced by the protons in making its path across the membrane is simply the sum of the two individual resistances.

Diffusion of protons through the composite membrane can be assumed to be a series of resistances of pure SPS and the porous membrane with SPS in the pores.

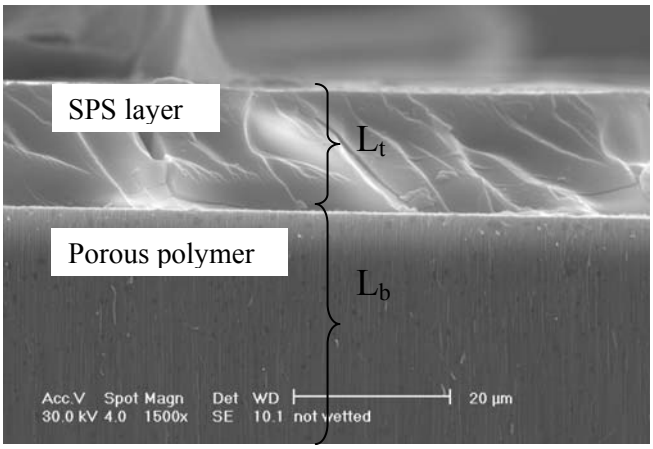

Figure 3.8 SEM of the cross-section of a composite membrane.

R_1 is the resistance of the SPS layer, R_2 is the resistance of the porous membrane with SPS in the pores, and R is the total resistance:

$$R=R_1+R_2 \; ; \; R_1=L_1/\kappa_1 A; \; R_2=L_2/\kappa_2 A$$

where L_1 and L_2, and κ_1 and κ_2 are the corresponding thicknesses and conductivities of the SPS and porous membrane with SPS in its pores, respectively. A is the area of the electrode through which current passes. The conductivity for the composite (κ) is given as:

$$\kappa=(L_1+ L_2)/[A(R_1+ R_2)]=(L_1+ L_2)/(L_1/\kappa_1+L_2/\kappa_2)$$

In the above equation, L_2, A, κ_1 are parameters that can be measured easily. That leaves κ to be a function of only L_1 and κ_2. This is a very important result that simply implies that the overall conductivity of the composite membrane is a function of the thickness of the SPS layer on top and the conductivity of the porous membrane with its pores filled. If an assumption is made regarding the conductivity of the porous membrane with its pores filled, that leaves the overall conductivity to be a function of only the thickness of the SPS layer on top of the porous membrane. Figure 3.9 gives a relationship between the

overall membrane conductivity as a function of the thickness of the conductive polymer layer on top of the porous membrane.

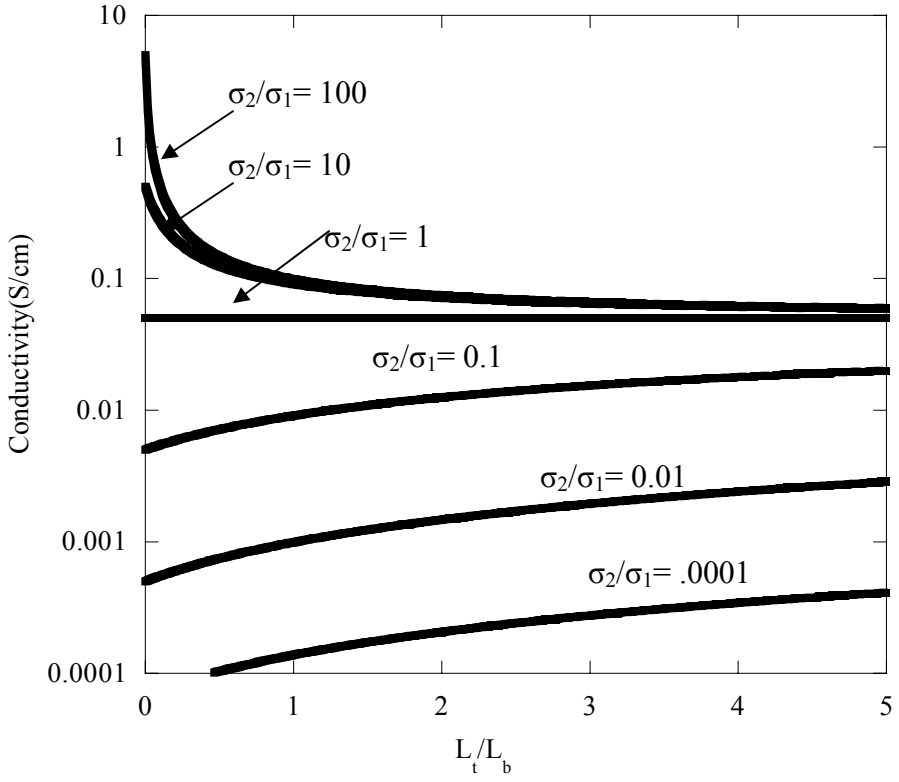

Figure 3.9 Conductivity versus L_t/L_b and varying conductivity ratios. σ_2 represents conductivity of polymer-filled matrix, and σ_1 represents conductivity of SPS.

The plot shows that at the value of L_t/L_b less than 2, the conductivity will either be high (if the filled porous membrane is more conductive than pure conductive polymer itself), or low (if the filled porous membrane is less conductive than pure conductive polymer). This graph gives an important result which tells us that (1) conductivity is a function of the ratio of thicknesses and conductivity of the nanopore-filled membrane, (2) at $L_t/L_b<1$:

conductivity of nanopore-filled membrane is the limiting factor, and (3) increasing pore-filling efficiency should increase conductivity at $L_t/L_b<1$.

3.4 Vacuum filtration

Vacuum filtration employs a pressure gradient that forces the polymer solution to fill the pores of the porous host membrane. As shown in Figure 3.10, PCTE or alumina membranes were placed on top of the stainless steel mesh holder. Five drops of solvent were poured on top of the membranes while applying vacuum.

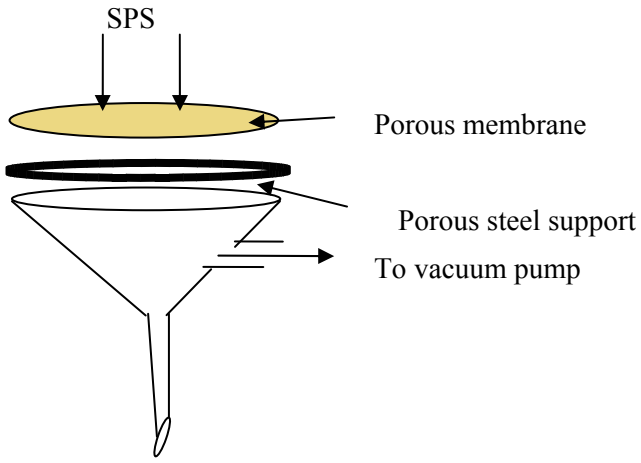

Figure 3.10 Schematic representation of the vacuum filtration process.

Fifteen drops of the polymer solution were then poured on top of the membrane while applying vacuum. The vacuum was pulled for a specified amount of time. The vacuum was stopped after the specified time interval and the membrane was removed carefully.

The filtered membranes were dried in a vacuum oven at 100^{o}C for 1 day. Filtered membranes were either spuncoat or blotted to reduce their thickness. It was observed that the pores were being filled (Figure 3.11 (a)), but again thick composites were being formed (L_t/L_b >>1) (Figure 3.11 (b)).

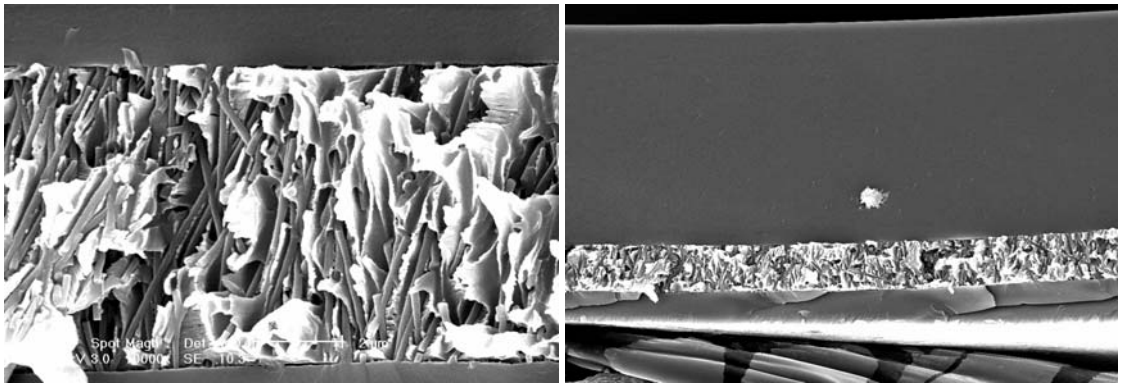

(a) (b)

Figure 3.11 SEM images of (a) SPS nanorods in the pores, (b) the composite is L_t/L_b >>1.

3.5 Vacuum filtration and spincoating

The effect of spincoating on the filled pores of PCTE was investigated in order to reduce L_t/L_b. A total of eight membranes were filtered using a 5 % (w/v) solution of SPS in acetone according to the filtration procedure described earlier. The filtered membranes were then spuncoat according to the procedures described in the section 2.2 by adding DMSO to the composite membrane surface and spincoating after a series of different

dissolution contact times. All membranes were freeze fractured in liquid nitrogen and SEM analysis was performed before and after spincoating.

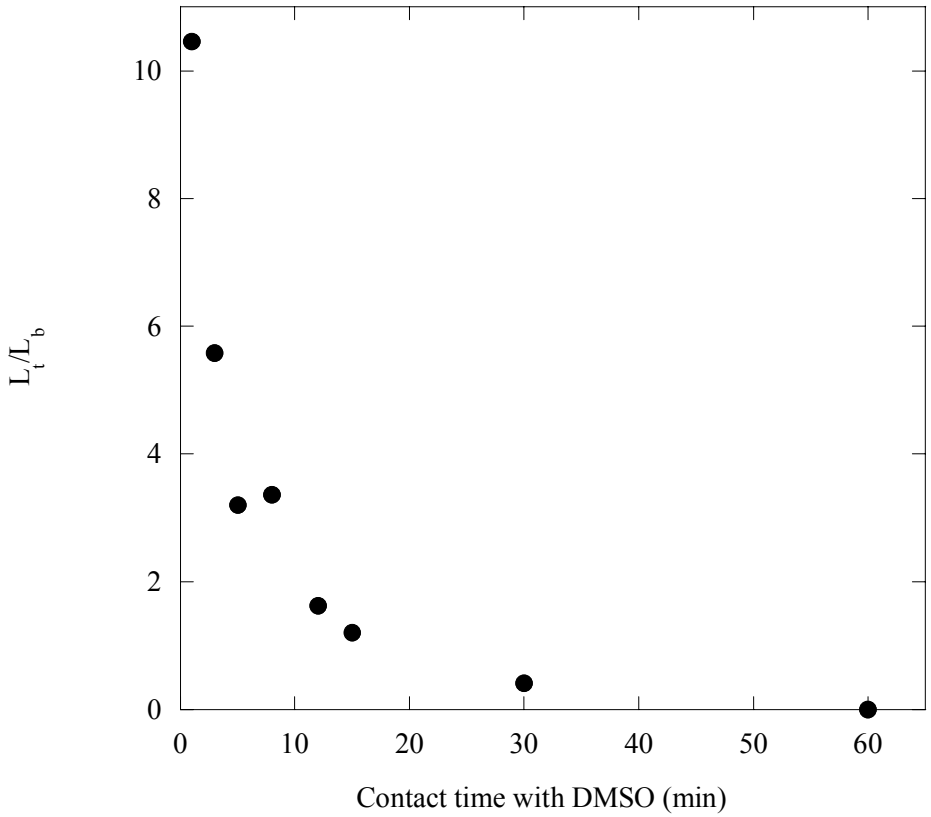

Figure 3.12 Thickness versus contact time with DMSO for spuncoat membranes.

Figure 3.12 is a plot of L_t/L_b of the composite membranes and contact time with DMSO. The plot shows that the thickness of the composites is reduced with increasing contact times. A L_t/L_b ratio of 10.46 is obtained for a contact time of 1 minute, and a L_t/L_b ratio of approximately 0 is obtained for 60 minutes. L_t/L_b =0 corresponds to no thickness of SPS on top of the PCTE membrane. SEM was conducted before and after spincoating to determine the effect on the composite. (Figure 3.13). Figure 3.13 (a), (c), (e), (g), (i), (k),

(m), and (o) show the presence of SPS nanorods within the PCTE template after filtration but before spincoating was performed.

(a)

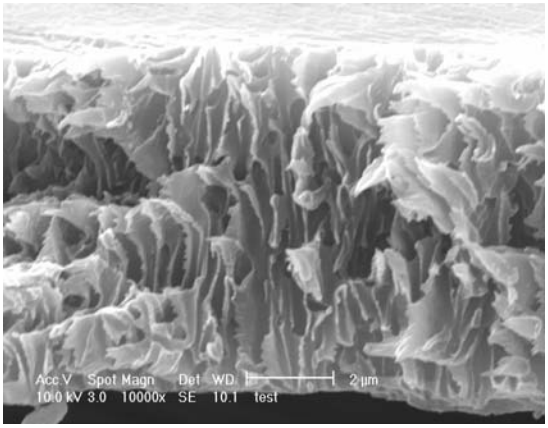

(b)

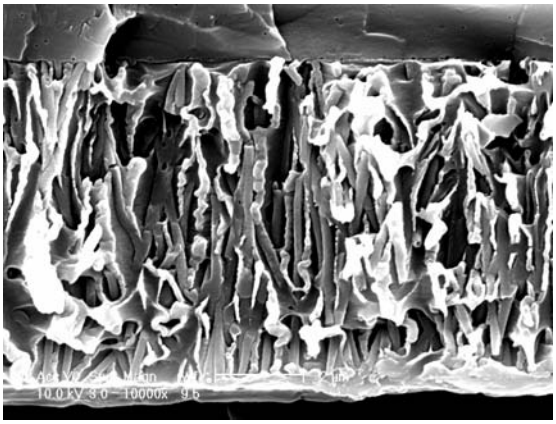

(c)

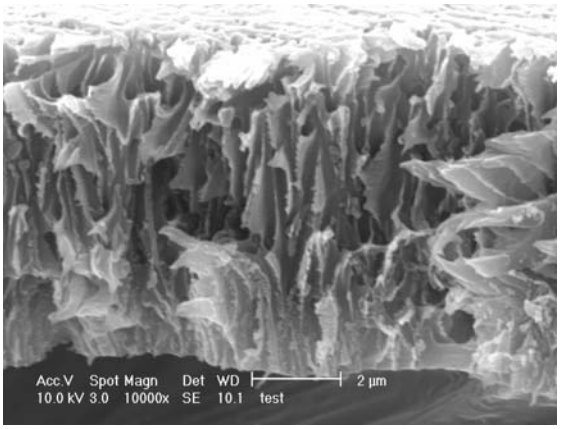

(d)

Figure 3.13 (a), (c), (e), (g), (i), (k), (m), and (o) SEM images of filtered PCTE membranes (100 nm pore size). (b), (d), (f), (h), (j,) (l), (n) and (p) SEM images of filtered and spuncoat PCTE membranes.

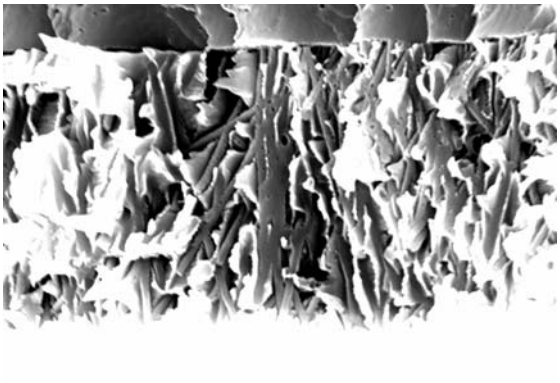

(e)

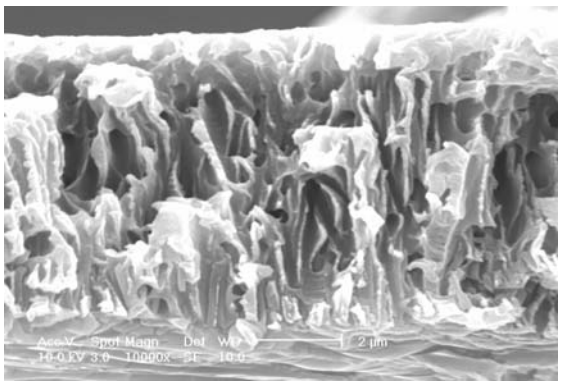

(f)

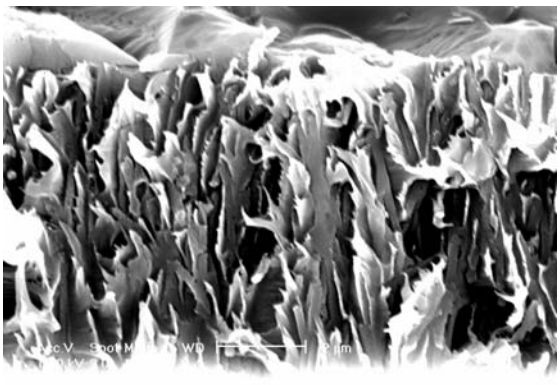

(g)

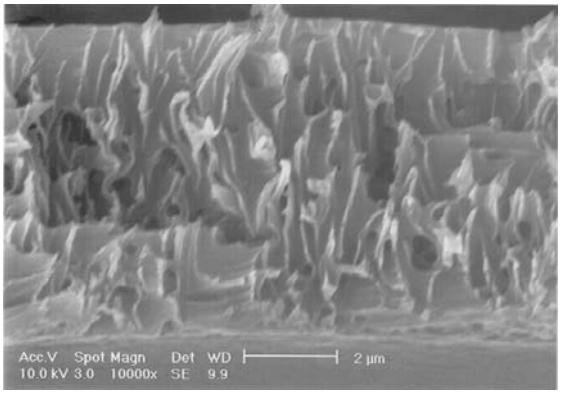

(h)

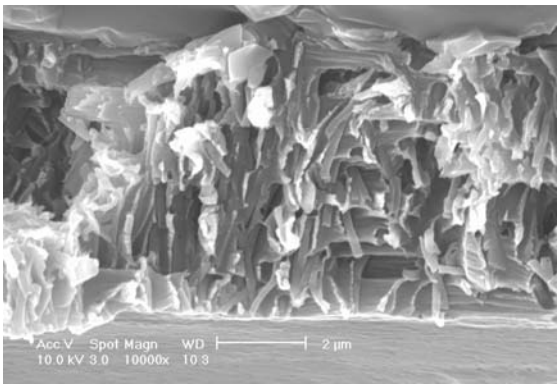

(i)

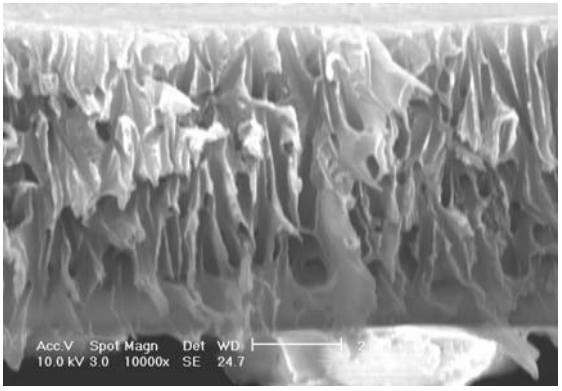

(j)

Figure 3.13 *(continued)*

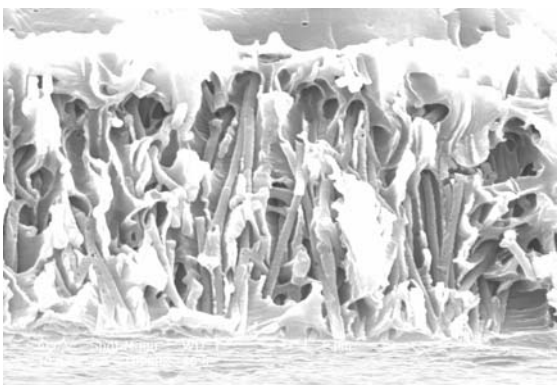

(k)

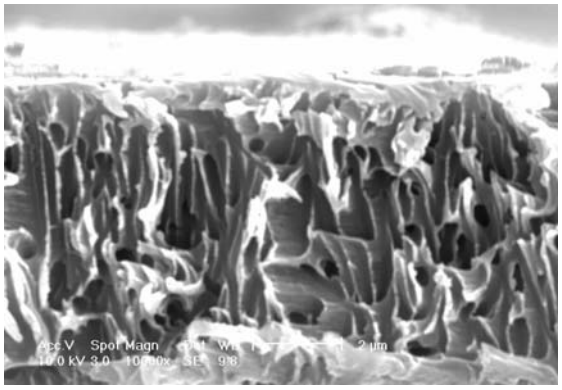

(l)

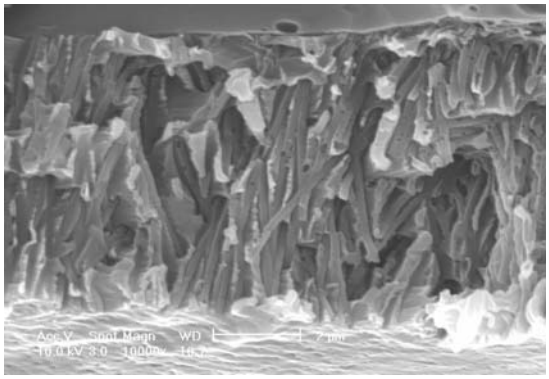

(m)

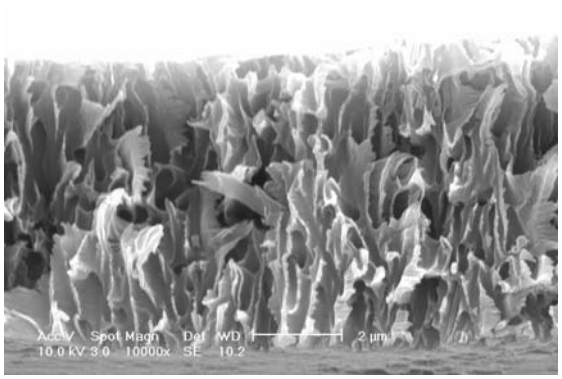

(n)

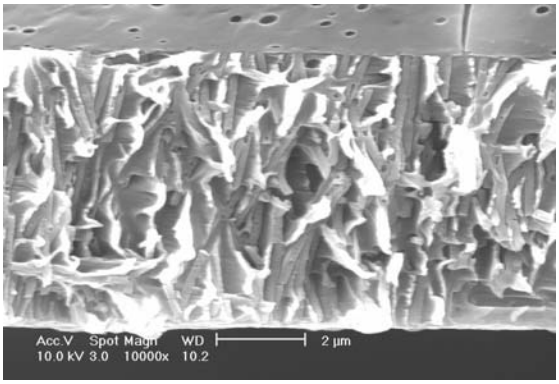

(o)

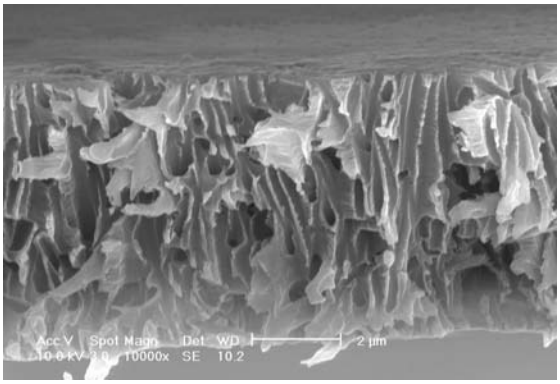

(p)

Figure 3.13 *(continued)*

Figure 3.13 (b), (d), (f), (h), (j), (l), (n) and (p) show that the pores of the PCTE membranes are empty. These SEM images were taken after spincoating was performed. It

can be concluded from the SEM images that before filtration, the pores of the host PCTE membranes were filled, whereas after spincoating, although the thickness was reduced, the pores were empty. AC Impedance spectroscopy was performed on the filtered and spuncoat membranes to measure conductivity. From Figure 3.14, it can be seen that conductivity increases with increasing thickness of the membranes. The value of conductivity is 1.62 x 10^{-5} S/cm at L_t/L_b=1.333 and increases to 4.45 x 10^{-5} S/cm at L_t/L_b=2.000. The conductivity increases three times as the thickness increases 1.5 fold. The magnitude of these conductivities confirm that no SPS is in the pores of the PCTE membrane after spincoating.

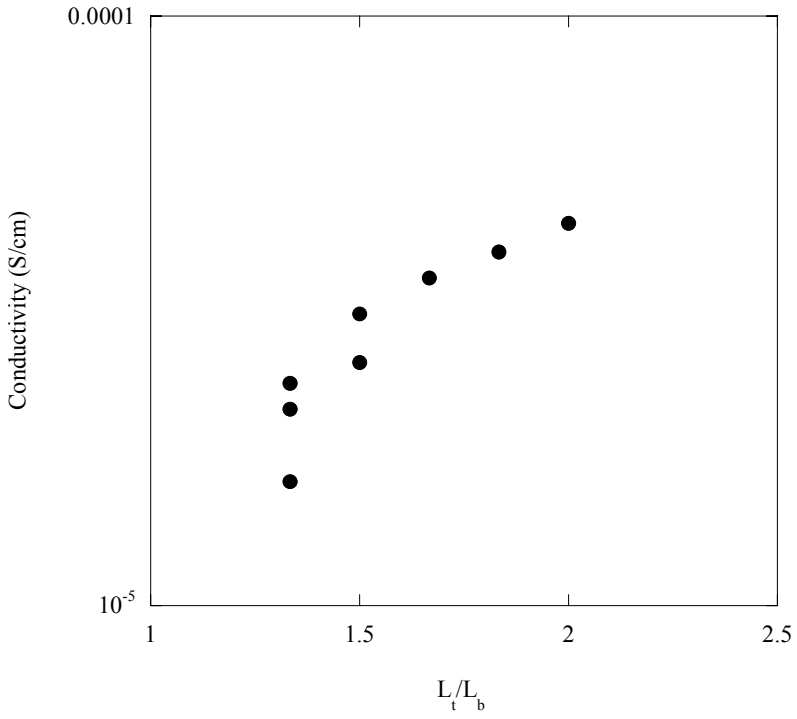

Figure 3.14 Conductivity versus L_t/L_b for filtered and spuncoat SPS/PCTE membranes.

3.6 Vacuum filtration and blotting

A new method of reducing the thickness of the polymer-filled membranes had to be devised that did not remove the polymer from within the pores of the PCTE membranes. Just after vacuum filtration was complete, excess polymer solution on both the sides of the membrane was gently blotted with a soft tissue. To study the effects of blotting on the filled pores, a study on eight membranes was performed. The eight PCTE membranes were first filtered with the SPS solution and a blotting step was performed on the membranes just after filtration.

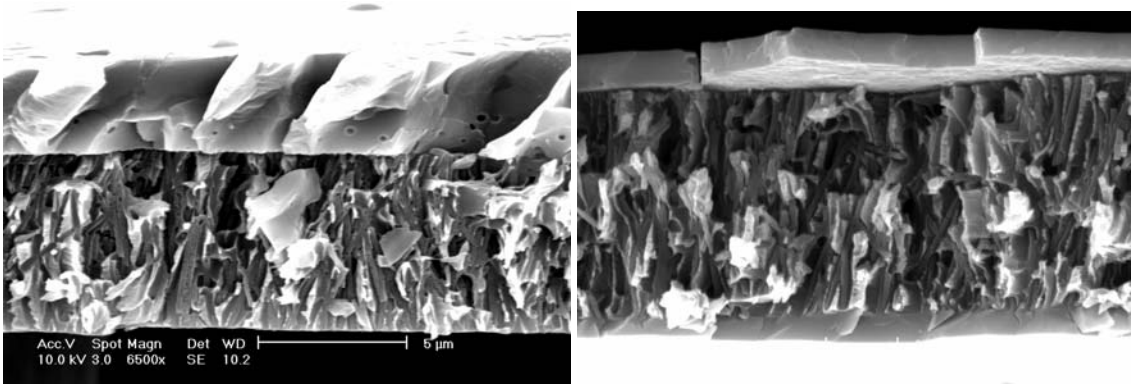

(a) (b)

Figure 3.15 SEM images of filtered and blotted SPS/PCTE membranes (100 nm pore size).

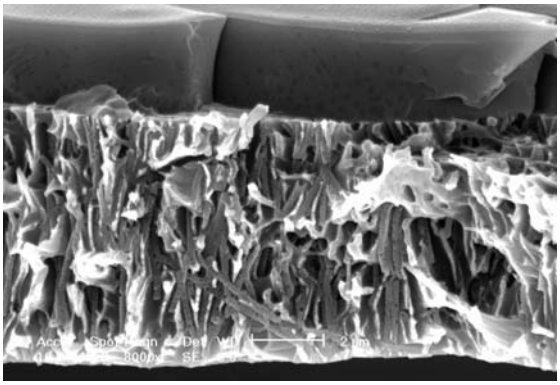

(c)

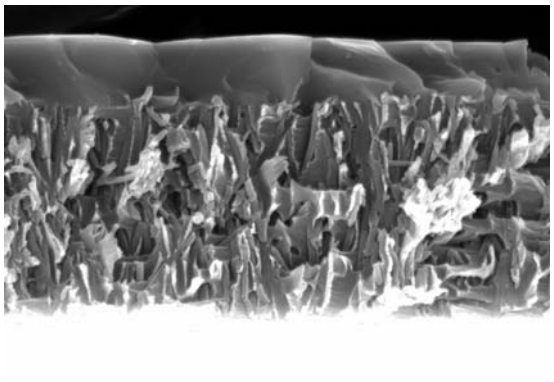

(d)

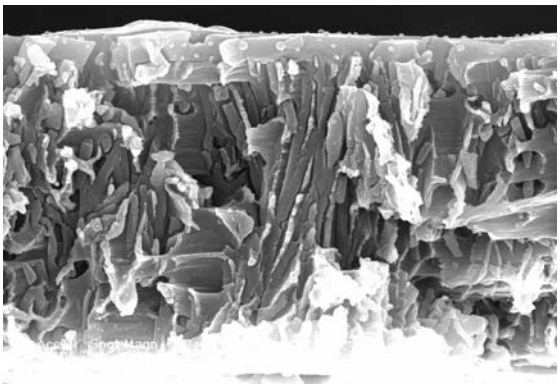

(e)

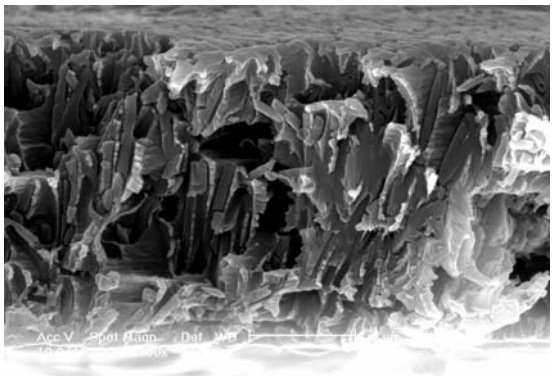

(f)

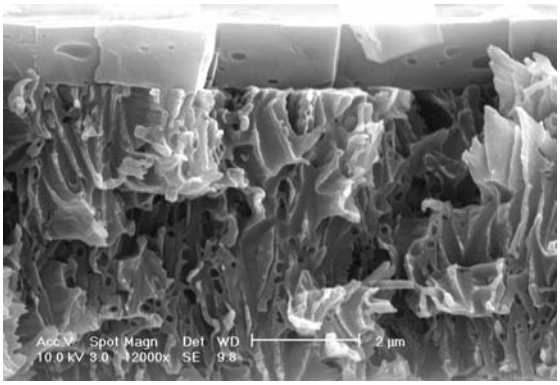

(g)

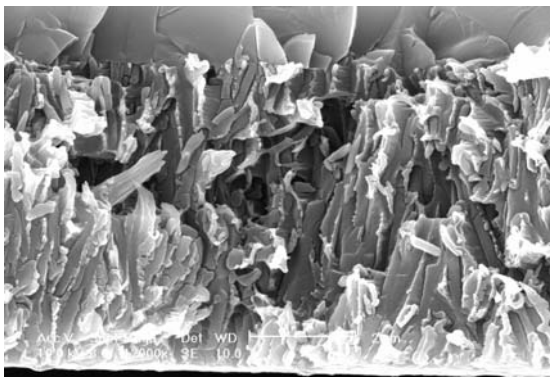

(h)

Figure 3.15 *(continued)*

It can be seen from Figure 3.15 that the thickness is reduced and filled polymer inside the pores is not affected by the blotting process. The difference between the spuncoat membranes and the blotted membranes is essentially that the pores of the blotted membranes are filled, whereas the pores of the spuncoat membranes are empty.

A study was performed to measure the conductivity of filtered and blotted membranes and compared to the conductivities of the filtered and spuncoat membranes. Figure 3.16 shows that conductivities of the blotted membranes were higher than conductivities of the spuncoat membranes by an order of magnitude.

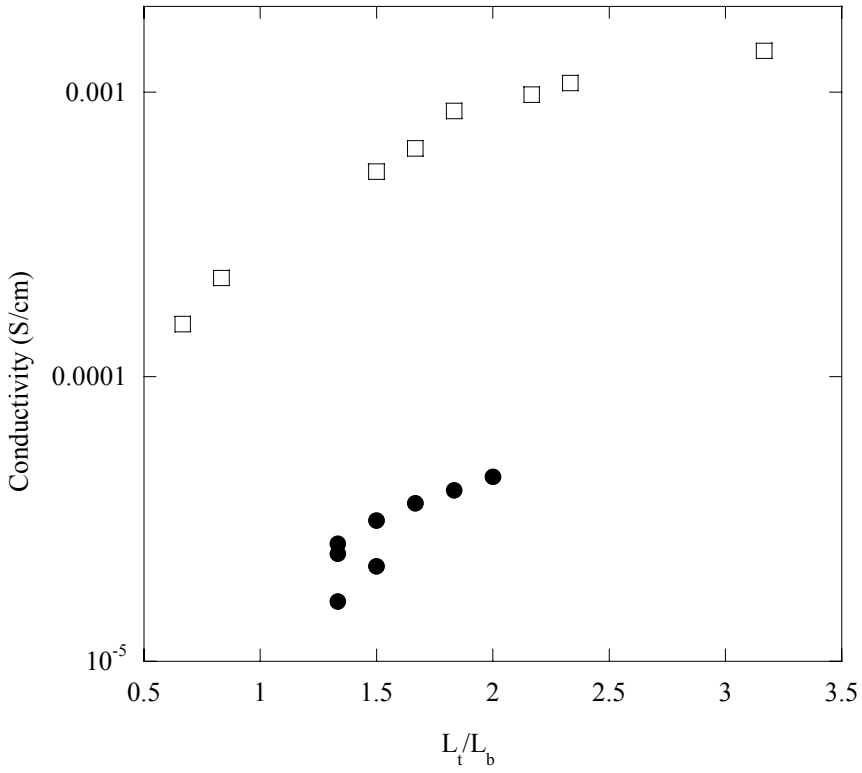

Figure 3.16 Conductivities of filtered and spuncoat (●) versus filtered and blotted (□) SPS/PCTE membranes (100 nm pore size).

At a value of L_t/L_b= 1.6667, the conductivity of the blotted membrane is 6.34 x 10^{-4} S/cm. At the same value of L_t/L_b, the conductivity of the spuncoat membrane is 3.6000 x 10^{-5} S/cm. This value is higher by more than an order of magnitude. At L_t/L_b=1.833, the value of conductivity for the blotted membrane is 8.60 x 10^{-4} S/cm, whereas for the spuncoat membrane, it is 3.9800 x 10^{-5} S/cm. The same trend of higher conductivities for blotted membranes is followed at comparable L_t/L_b ratios.

3.6.1 Fabrication of SPS-PCTE composites (50 nm pore size)

Composites of SPS-PCTE (50 nm pore size) were fabricated using the vacuum filtration and blotting procedure. The following SEM images of the membrane cross-sections were obtained. Figure 3.17 shows that pores of PCTE (50 nm pore size) membranes are filled with nanorods of SPS.

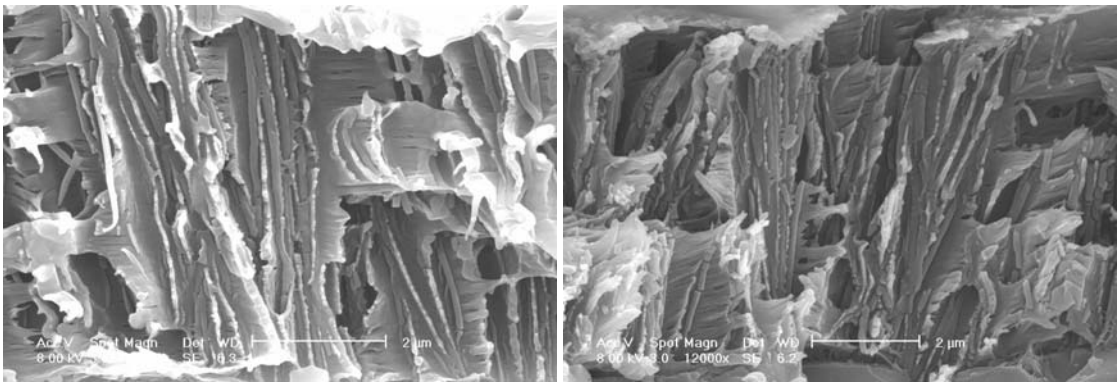

(a) (b)

Figure 3.17 SEM images of filtered and blotted PCTE membranes (50 nm pores size).

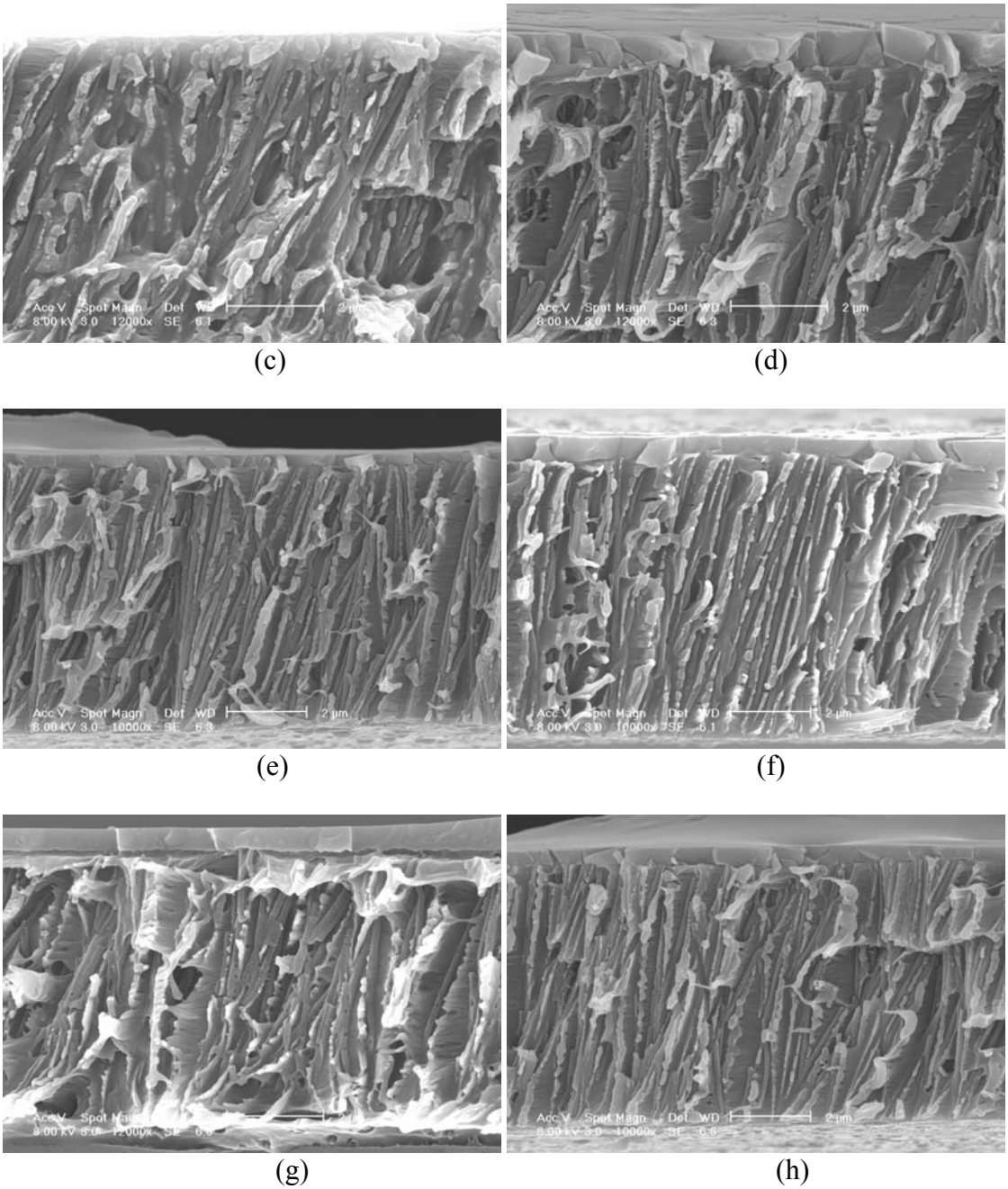

(c) (d)

(e) (f)

(g) (h)

Figure 3.17 *(continued)*

The thicknesses of these membranes were reduced to $L_t/L_b < 1$ using blotting. The conductivities of these membranes were measured using EIS and the results are shown in

Figure 3.18. The conductivities of the SPS-PCTE 50 nm (pore size) membranes were measured using EIS.

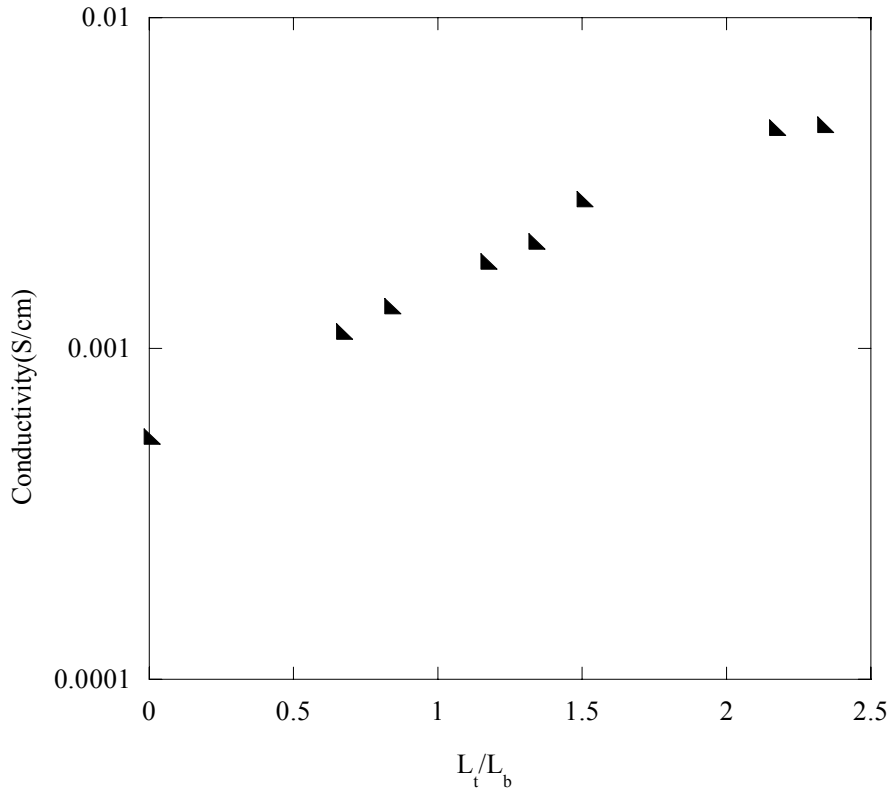

Figure 3.18 Conductivity versus L_t/L_b for SPS-PCTE (50 nm pore size) composites.

Figure 3.18 shows that conductivity increases as the thickness of the composites increases. A conductivity of 5.41 x 10^{-4} S/cm is obtained for L_t/L_b=0 and the conductivity increases to a value of 4.7600 x 10^{-3} S/cm for L_t/L_b=2.333. The conductivity at L_t/L_b=0 is 3.1925 x 10^{-4} S/cm, which is approximately two orders of magnitude lower than pure SPS and one order of magnitude higher than empty PCTE (50 nm pore size).

3.6.2 Fabrication of SPS-alumina composites (100 nm pore size)

Composites of SPS-alumina (100 nm pore size) were fabricated using vacuum filtration and blotting. As before, the alumina 100 nm membranes were filtered with a 5 % (w/v) solution of SPS /acetone. After filtration, the membranes were briefly blotted to remove excess SPS solution from the membrane. The membranes were dried in a vacuum oven at 100^{o} C for 1 day. Eight such membranes were fabricated. The membranes were freeze fractured in liquid nitrogen, mounted on stubs, sputter-coated with Pt, and SEM was performed. The following SEM images of the membrane cross-sections were obtained (Figure 3.19).

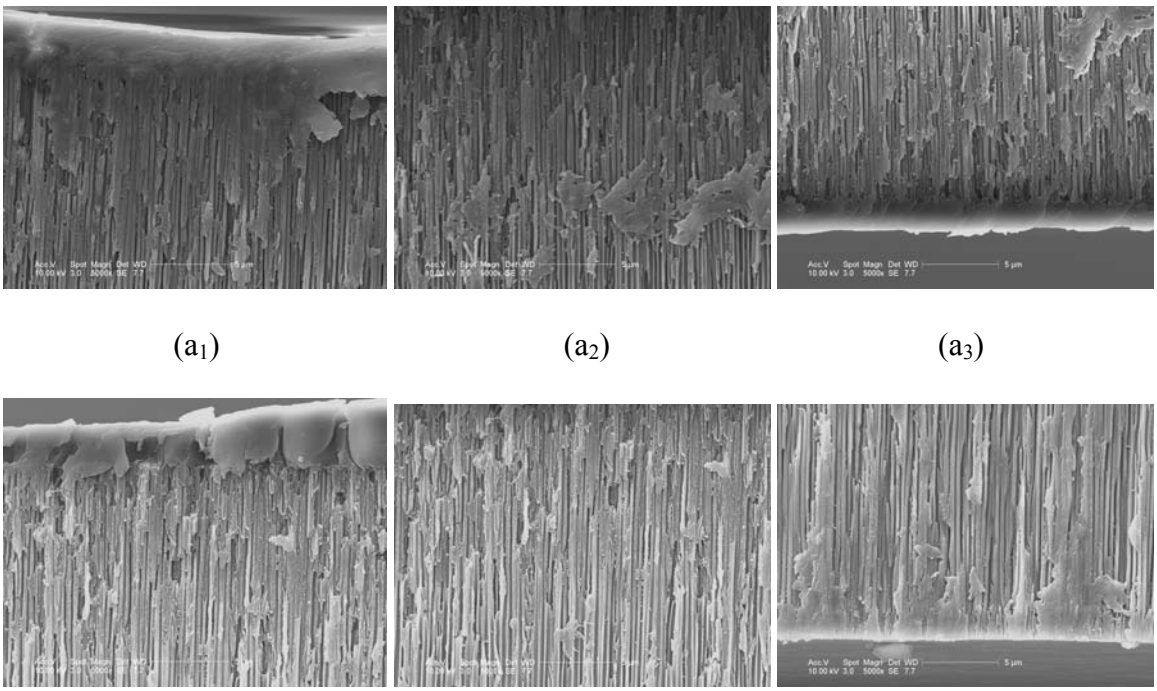

(a_1) (a_2) (a_3)

(b_1) (b_2) (b_3)

Figure 3.19 SEM images of filtered and blotted (100 nm pore size) alumina membranes. Subscripts 1, 2 and 3 refer to top, middle and bottom sections, respectively.

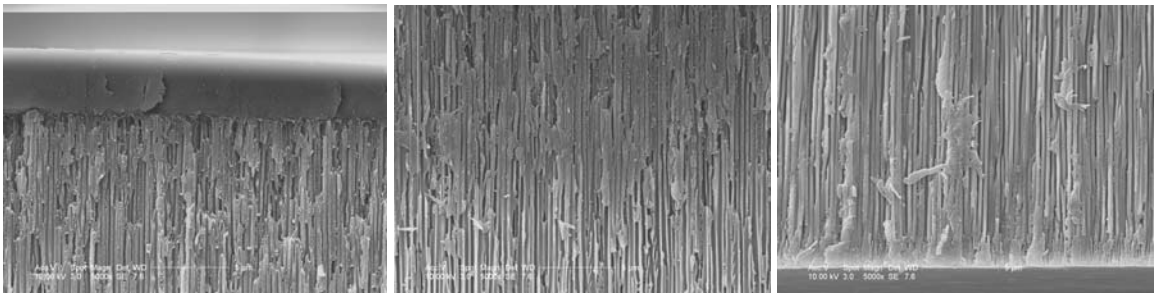

(c_1) (c_2) (c_3)

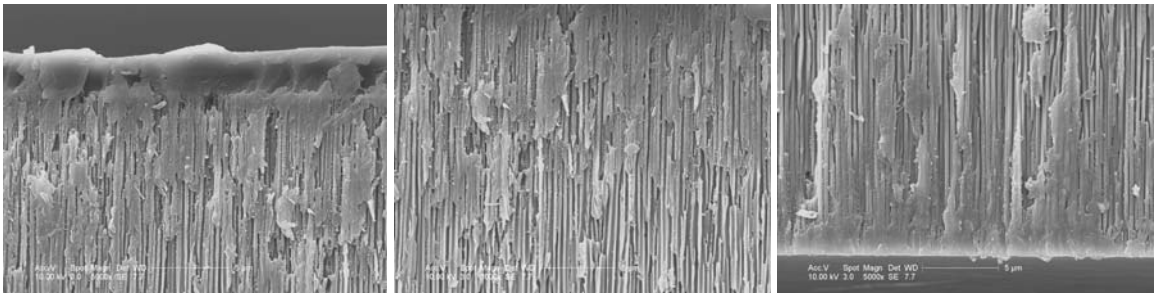

(d_1) (d_2) (d_3)

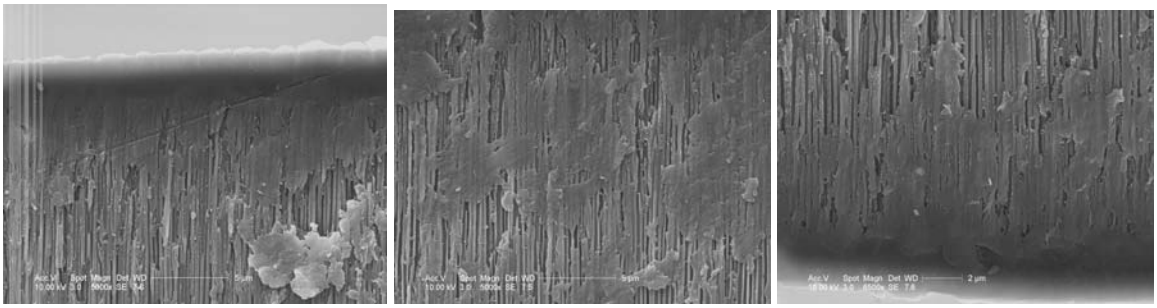

(e_1) (e_2) (e_3)

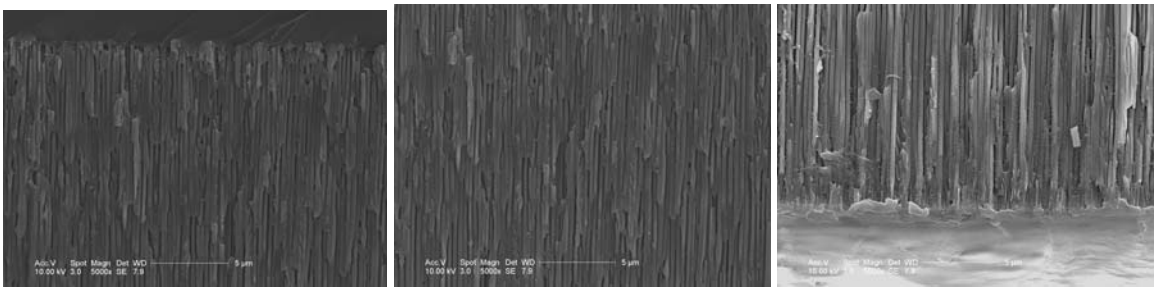

(f_1) (f_2) (f_3)

Figure 3.19 *(continued)*

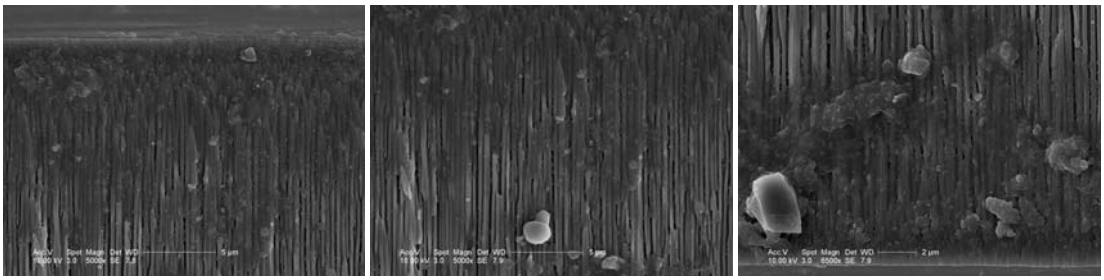

(g_1) (g_2) (g_3)

(h_1) (h_2) (h_3)

Figure 3.19 *(continued)*

The conductivities of the SPS-alumina 100 nm (pore size) membranes were measured using AC impedance spectroscopy. From Figure 3.20, it is seen that the value of conductivity is 1.3430 x 10^{-3} S/cm at L_t/L_b= 0.24138, and the conductivity increases to 7.9318 x 10^{-3} S/cm at L_t/L_b= 0.55172. This is a 6-fold increase in the value of conductivity for a 2-fold increase in the value of thickness.

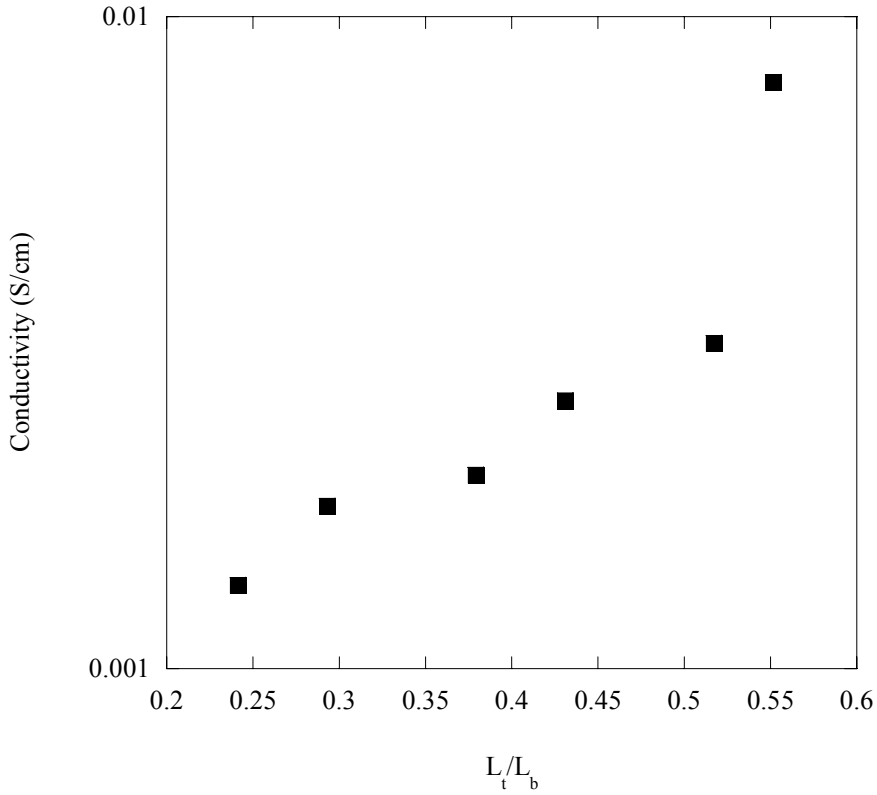

Figure 3.20 Conductivity versus L_t/L_b for SPS/alumina (100 nm pore size) composite membranes.

3.6.3 Fabrication of SPS-alumina composites (20 nm pore size)

Composites of SPS-Alumina 20 nm were fabricated using vacuum filtration and blotting, using the same procedure as SPS/Alumina composites (100 nm pore size). The following SEM images of the membrane cross-sections were obtained (Figure 3.21)

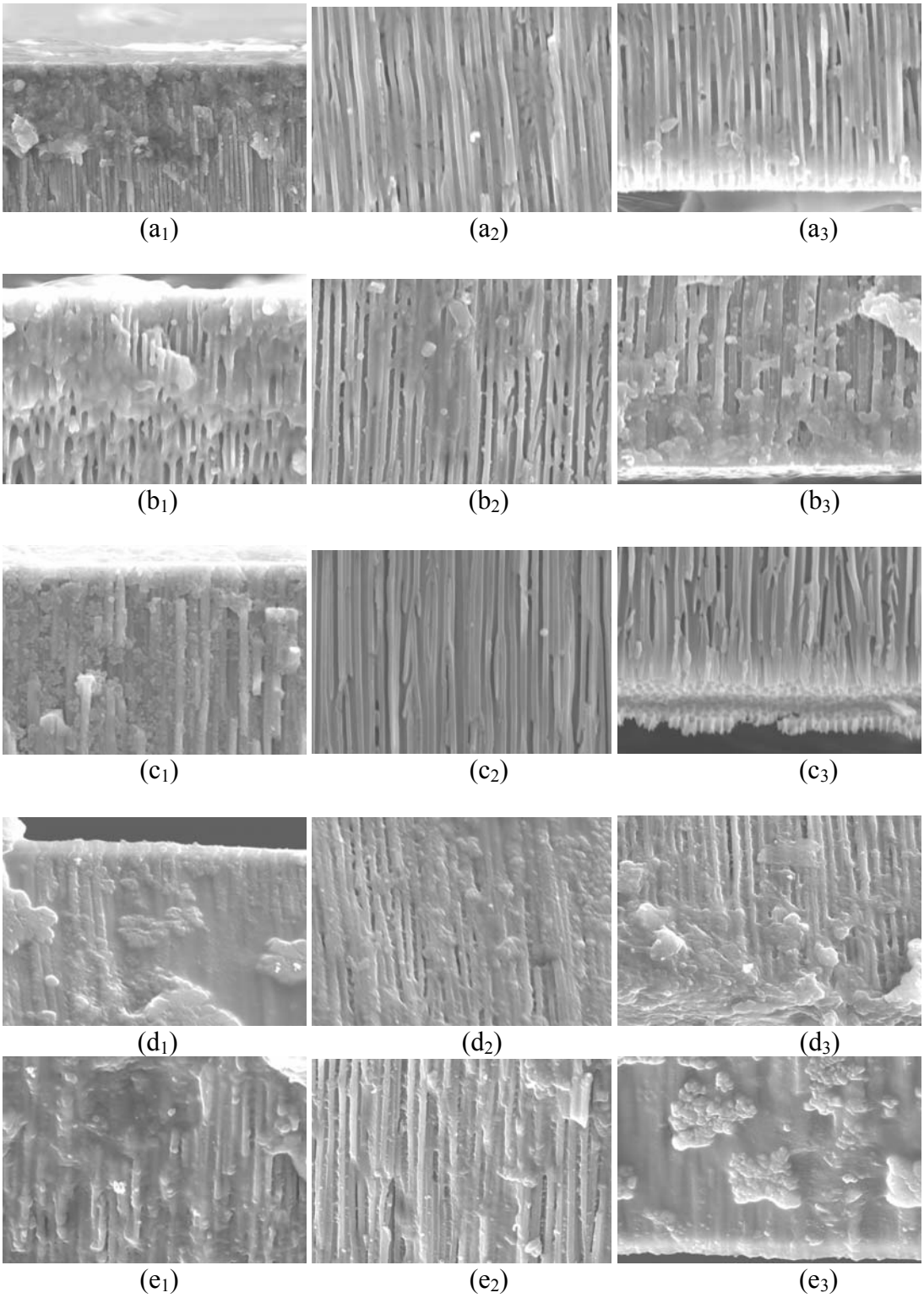

Figure 3.21 SEM images of filtered and blotted SPS/alumina composites (20 nm pore size). Subscripts 1, 2 and 3 refer to top, middle and bottom sections, respectively.

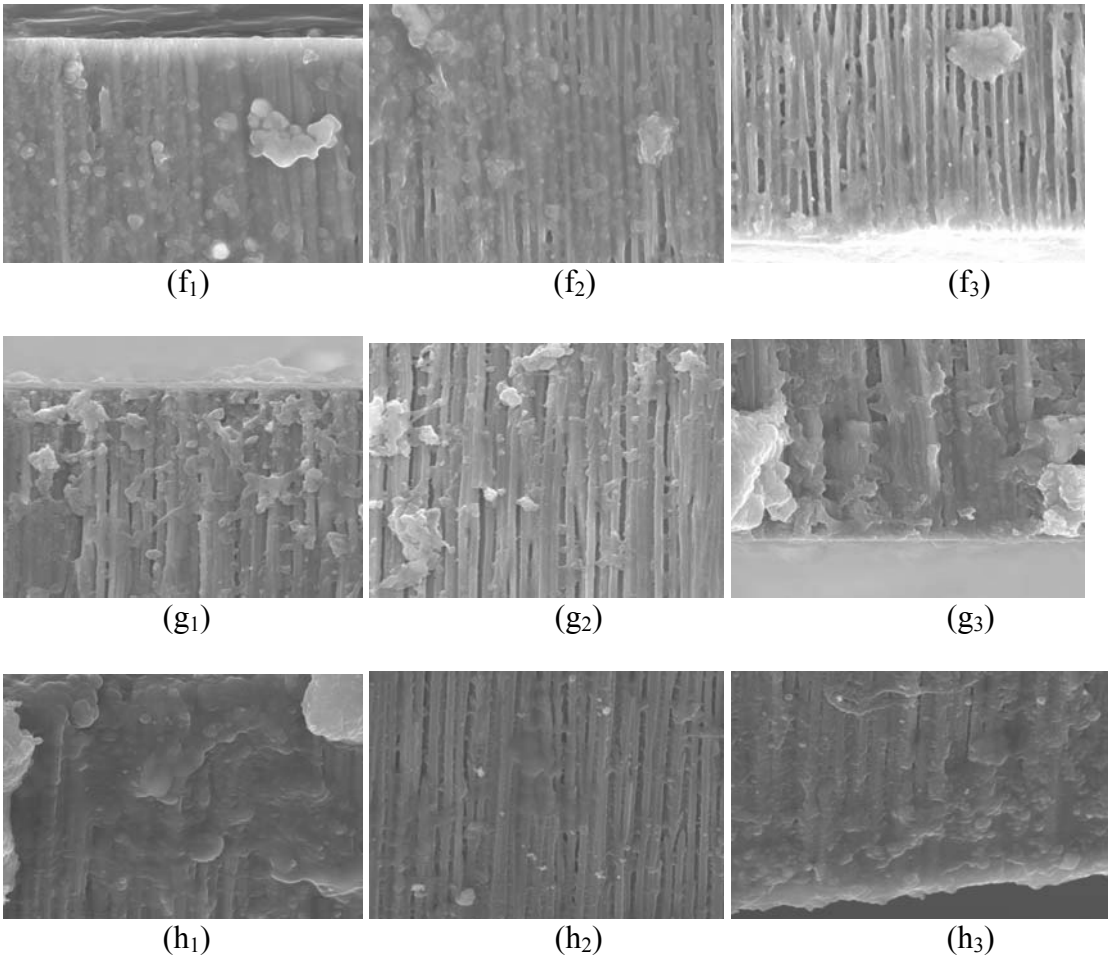

(f_1) (f_2) (f_3)

(g_1) (g_2) (g_3)

(h_1) (h_2) (h_3)

Figure 3.21 (*continued)*

Figure 3.21 shows that pores of SPS/alumina (20 nm pore size) membranes filled with SPS. The thickness of these membranes was reduced to $L_t/L_b < 1$ using blotting. The conductivities of these membranes were measured and the results are shown in Figure 3.22. Experiments on only six of the eight fabricated membranes could be performed because the membranes were extremely fragile and broke in handling.

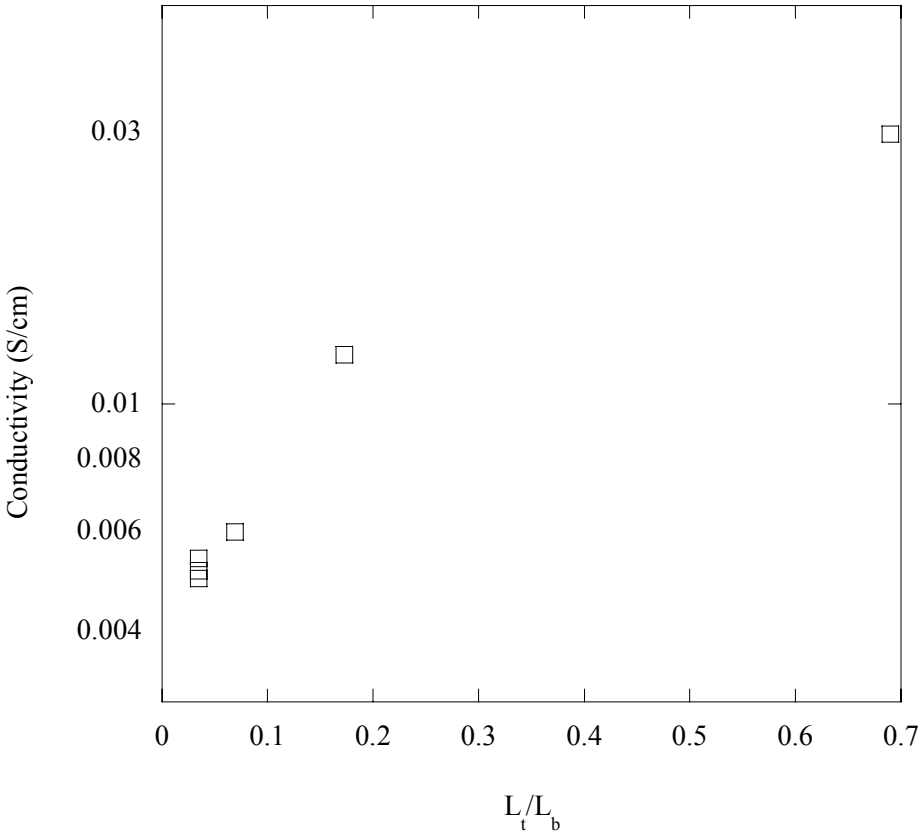

Figure 3.22: Conductivity versus L_t/L_b for SPS/alumina composites (20 nm pore size).

Figure 3.22 shows that conductivity increases as the thickness of the composites increase. A conductivity of 5.094 x 10^{-3} S/cm is obtained for L_t/L_b=3.4483 x 10^{-2} and the conductivity increases to a value of 2.979 x 10^{-3} S/cm for L_t/L_b=0.689.

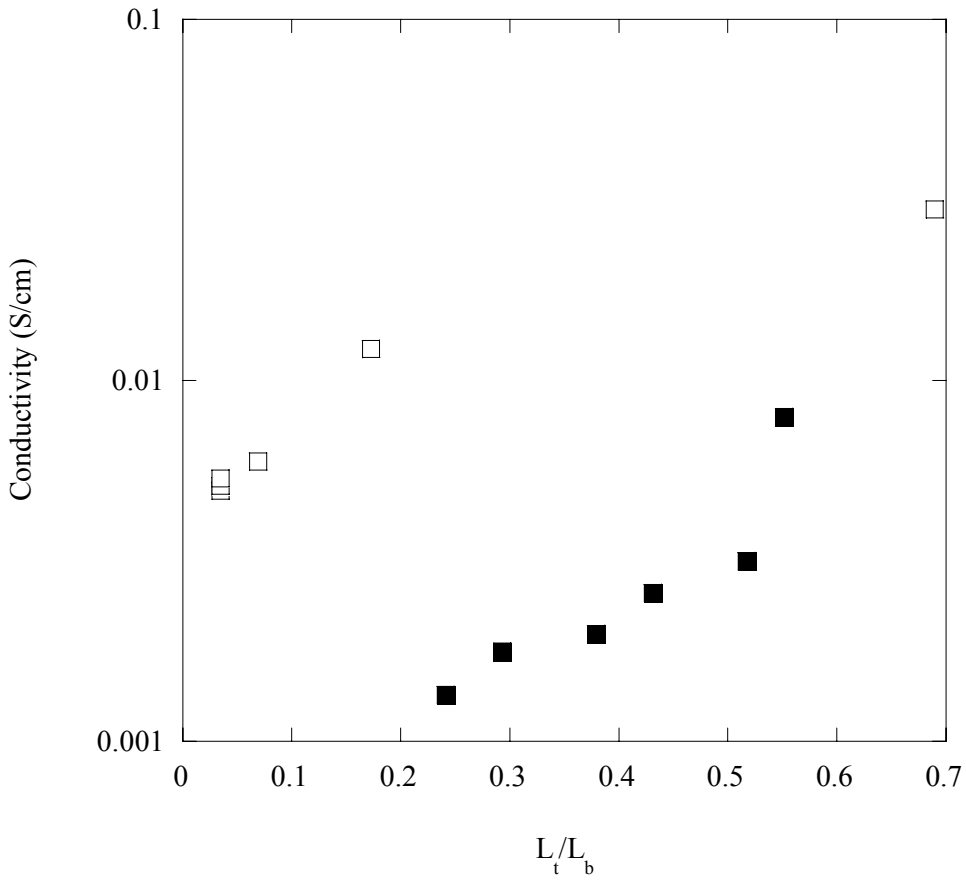

Figure 3.23 Comparison of conductivities of SPS/Alumina (100 nm pore size,■) and SPS/Alumina (20 nm pore size, □) composite membranes.

From Figure 3.23, it can be seen that the conductivities of SPS/alumina composites (20 nm pore size) are higher by approximately an order of magnitude than the conductivities of SPS/ alumina composites (100 nm pore size) over the same thickness range.

CHAPTER 4: ANALYSIS

4.1 Effect of thickness, pore size and pore density

Figure 4.1 is a plot that summarizes the conductivity data for the fabricated membranes. The membranes fabricated were filtered and spuncoat SPS/PCTE (100 nm pore size), filtered and blotted SPS/PCTE (100 nm pore size), filtered and blotted SPS/PCTE (50 nm pore size), filtered and blotted SPS/alumina (100 nm pore size) and filtered and blotted SPS/alumina (20 nm pore size). In addition, the plot also shows the conductivities of the host membranes: PCTE (100 nm, 50 nm and 10 nm pore sizes), Alumina (100nm and 20 nm pore sizes). A number of conclusions can be drawn from Figure 4.1

First, the conductivities of all the fabricated membranes are a function of thickness. This can be seen from the increasing values of conductivities with thickness for the fabricated membranes. The conductivity model presented in Chapter 3.3 explains this result mathematically. It can be seen that the conductivities of polymer-filled membranes are always higher than the conductivities of the corresponding host membranes. This trend is seen for all the polymer-filled membranes.

Second, conductivities are a function of the pore size of the host membrane. The conductivities of SPS/PCTE composites (50 nm pore size) are approximately 2-fold higher than conductivities of SPS/PCTE composites (100 nm pore size).

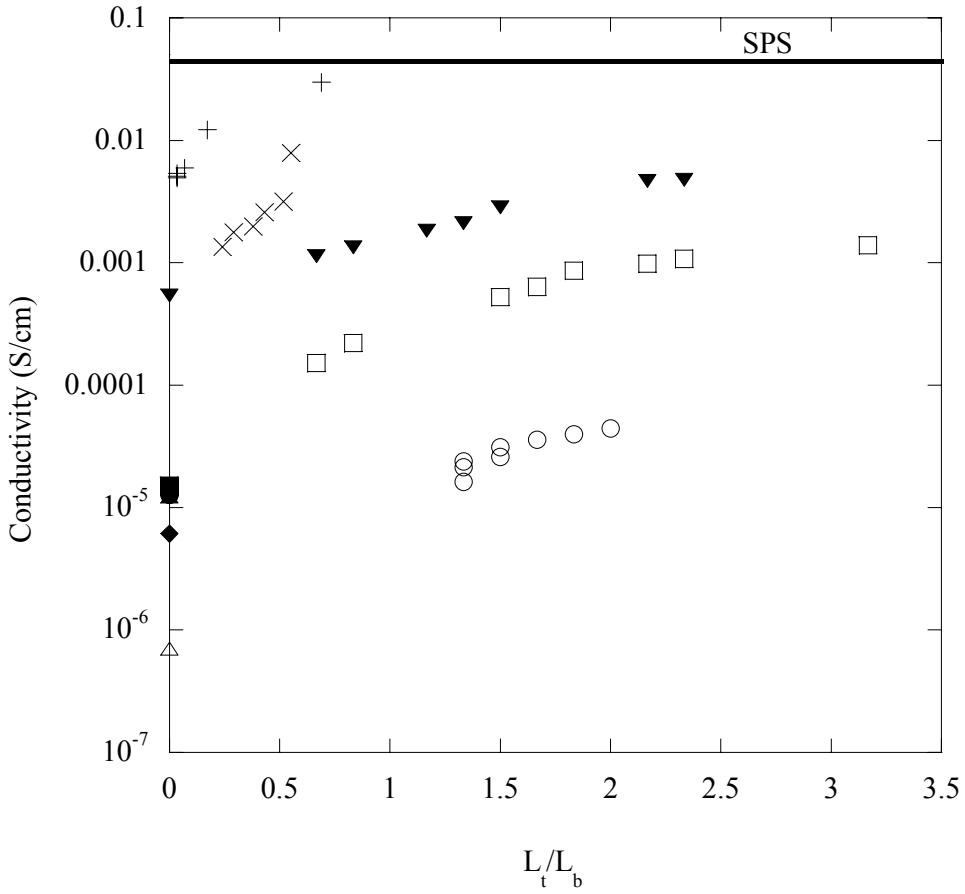

Figure 4.1 Conductivities of filtered and spuncoat SPS/PCTE (100 nm)(○), filtered and blotted SPS/PCTE (100 nm) (□), filtered and blotted SPS/PCTE (50 nm) (▼), filtered and blotted SPS/alumina (100 nm) (x), filtered and blotted SPS/alumina (20 nm) (+), PCTE (100 nm) (▲), PCTE (50 nm) (●), PCTE (10 nm) (Δ), alumina (100 nm) (♦), alumina (20 nm) (■).

Also, the conductivities of SPS/Alumina composites (20 nm pore size) are higher than conductivities of SPS/Alumina composites (100 nm pore size) by approximately an order of magnitude over the same thickness range. These trends can be explained on the basis of Figure 4.2. Ionic clusters are interconnected in PEMs, where the size is on the order of 10 nm. If the PEM is confined to pores greater than 100 nm in size, the network of ionic clusters within the pore would be unaffected. However, if the PEM was confined to pores approximately 10-100 nm in size, the network of ionic cluster would be constricted,

altering the ionic morphology. The ionic cluster network would be more aligned along the pore length. The paths for proton transport would then be less tortuous. This would enhance proton conductivity.

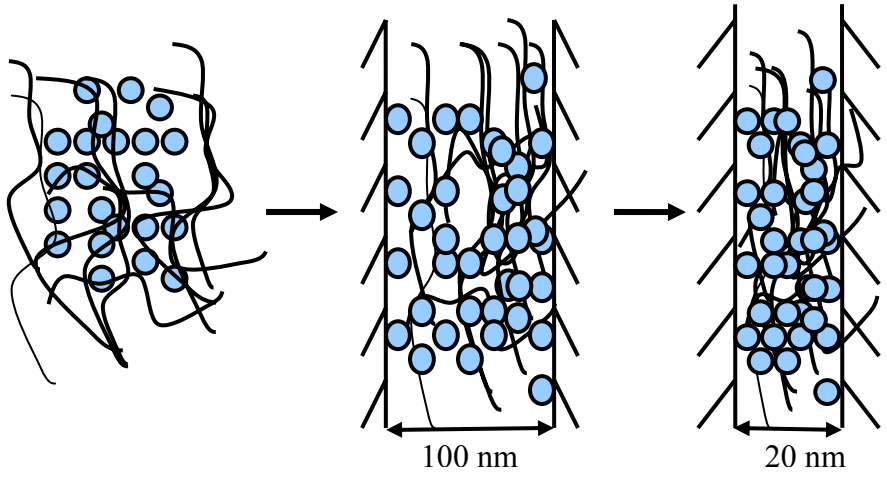

Figure 4.2 (a) Ionic clusters in a PEM not confined to a pore (b) Ionic clusters in a PEM confined to a 100 nm pore (c) Ionic clusters in PEM confined to a 20 nm pore.

Third, conductivities of SPS/Alumina (100 nm and 20 nm pore sizes) membranes are more conductive than the pore-filled SPS/PCTE composites (100 nm and 20 nm pore sizes). Alumina (50 % porosity) has a higher porosity than PCTE (0.1 % porosity). Maxwell's equation for effective diffusivity in a heterogeneous medium is:

$$(\sigma - \sigma_b)/(\sigma + 2\sigma_b) = v_a(\sigma_a - \sigma_b)/(\sigma_a + 2\sigma_b)$$

This equation relates the overall conductivity of the composite (σ) to the conductivity of the dispersed phase (σ_a) and conductivity of the continuum (σ_b) through athe volume fraction of the dispersed phase (v_a) that exits in the continuum. The effective conductivity, when integrated with the multilayer model (chapter 3.3), results in the lines shown in Figure 4.3. The model predicts that conductivities for SPS/alumina composites are higher than conductivities for SPS/PCTE composites. This prediction is confirmed by conductivities for SPS/alumina composites (100 nm and 200 nm pore sizes), which are higher than conductivities of SPS/PCTE composites (100 nm and 50 nm pores sizes) over the same thickness range.

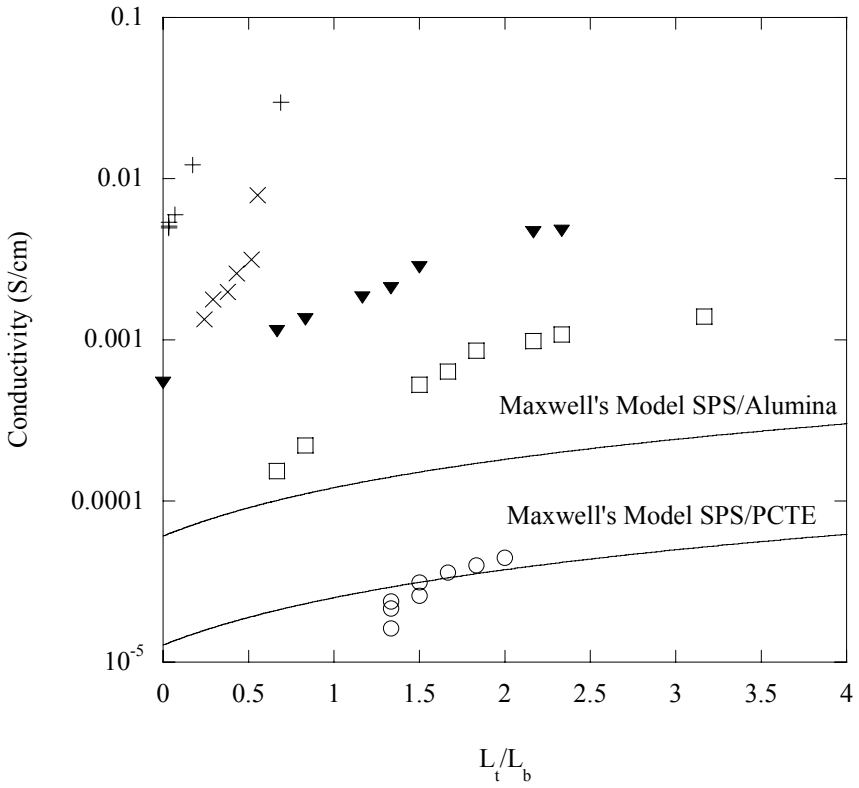

Figure 4.3 Conductivities of filtered and spuncoat SPS/PCTE (100 nm) (○), filtered and blotted SPS/PCTE (100 nm) (□), filtered and blotted SPS/PCTE (50 nm) (▼), filtered and blotted SPS/alumina (100 nm) (x), filtered and blotted SPS/alumina (20 nm) (+). The lines represent Maxwell's model for SPS/alumina and SPS/PCTE composites.

However, the combined Maxwell-series resistance model does not accurately coincide with the experimental data. This model accounts for the volume fraction and the thickness of the electrolyte, but does not account for the affect of pore size or ion content on the composite. A model that accounts for all of these factors must be developed to accurately match the experimental data.

4.2 Pore-filling analysis

Capillary flow rate in a tube is given by the Washburn equation:

$$U=\frac{r^2 x(\Delta P-P_c)}{(8x\mu effxd)}$$

where μeff is the effective viscosity, d is the length of tube, r is the radius of tube, ΔP is the pressure drop and P_c is the capillary pressure given by :

$$P_c=\frac{2\sigma\cos\theta}{R}$$

Where θ is the contact angle and σ is the surface tension. During natural sorption, the capillary pressure is not enough to provide a driving force to fill the pores with SPS solution. The additional force to achieve this is provided by vacuum that is applied by the pump. From Table 4.1, it can be seen that SPS/acetone solution had the least viscosity (least internal resistance to flow) and least contact angle (highest wetting capability) amont the filling solutions used. Hence the flow rate of SPS/acetone solution was the highest (see Washburn equation). Another important property of a polymer is radius of gyration.

The size of a macromolecule in solution is defined by its hydrodynamic radius. When pressure is applied and a macromolecule is brought near the pore of a membrane, the shape of the

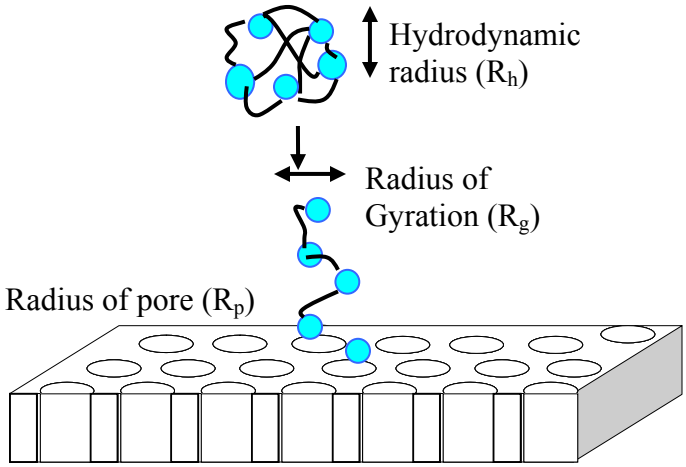

Figure 4.4 Schematic representation of a polymer chain entering a pore of a host membrane.

macromolecule changes to a random coil, and its size is then defined by radius of gyration. When the radius of gyration of the polymer is greater than the pore diameter, it is difficult to fill the pores of the host membrane (Figure 4.4). PS had a radius of gyration of 13.75 nm[33].

From the table, it can be seen that SPS/acetone has the least viscosity (4 cP), least contact angle (0^o) on PCTE and alumina surfaces. This meant that SPS/acetone solution presented the least internal resistance to flow inside the pores and had the highest wetting capability among the solutions. These results are in confirmation with the result that only

SPS/acetone solution was successfully able to fill the pores of the host membranes. SPS/acetone successfully filled the pores of PCTE (50 and 100 nm pore size) (Figures 3.15 and 3.17). SPS/acetone successfully filled the pores of Alumina (20 nm and 100 nm pore sizes) (Figures 3.19 and 3.21). SPS/acetone could only partially fill the pores of PCTE (10 nm pore size) (Figure 4.7). SPS/DMSO failed to fill the pores of the host membranes because of the comparatively high values of viscosity and contact angle. Nafion® (Ion Power) and Nafion® (Aldrich) failed to fill the pores of any of the host membranes.

Table 4.1 Summary of physical properties of solutions.

Solution	Viscosity (cP)	Contact Angle on PCTE	Contact Angle on Alumina
SPS/Acetone	4	0^o	0^o
SPS/DMSO	19	10.33^o	17.33^o
Nafion® (Ion Power)	8	14.875^o	16^o
Nafion® (Aldrich)	16	24.875^o	24.5^o

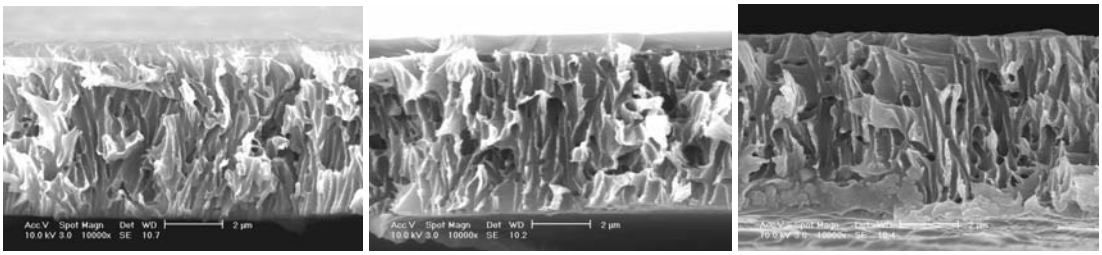

(a) (b) (c)

Figure 4.4 PCTE (100 nm pore size) membranes filtered with Nafion® (Ion Power)

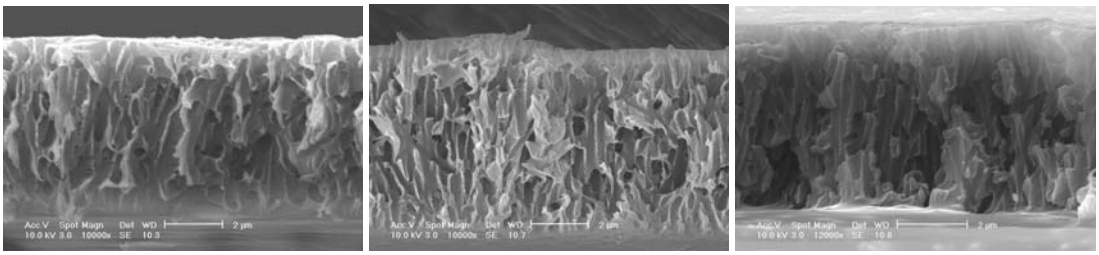

(a) (b) (c)

Figure 4.5 PCTE (100 nm pore size) membranes filtered with Nafion® (Aldrich)

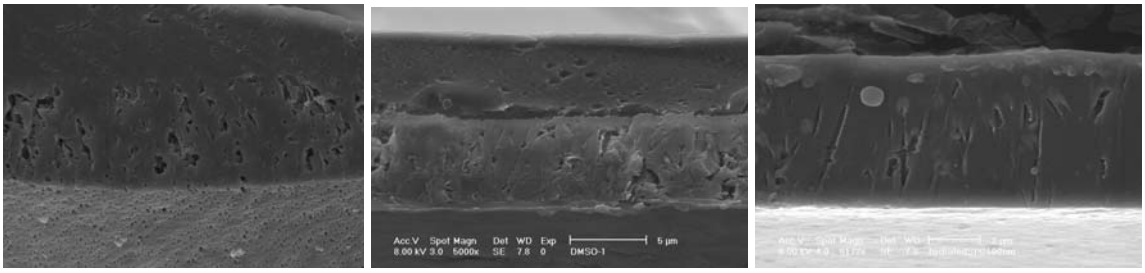

(a) (b) (c)

Figure 4.6 PCTE (100 nm pore size) membranes filtered with SPS/DMSO

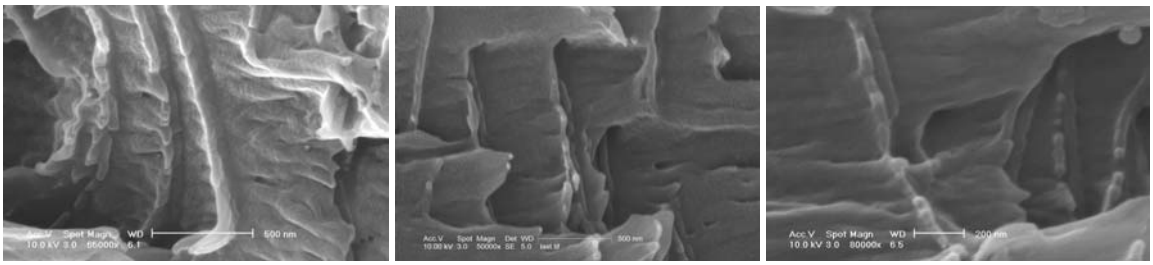

(a) (b) (c)

Figure 4.7 PCTE (10 nm pore size) membranes filtered with SPS/acetone

CHAPTER 5: CONCLUSIONS

The goal of this study was to fabricate polymer-filled nanoporous membranes and to study the conductivities of the fabricated membranes with respect to thickness, pore sizes and porosity of the membranes. The host membranes used in this study were PCTE (100 nm pore size), PCTE (50 nm pore size), PCTE (10 nm pore size), alumina (100 nm pore size) and alumina (20 nm pore size). The filling polymer was sulfonated polystyrene. The sulfonated polystyrene was determined to be 43 mol % sulfonated. Sorption and vacuum filtration were the two techniques used to fill the pores of the host membranes. The pores of the host membranes were successfully filled with vacuum filtration, whereas sorption proved to be an ineffective method to fill the pores. The thickness of the polymer-filled membranes was reduced using a blotting technique. The thickness of the membranes could be reduced using spincoating, but this technique removed the polymer from the pores of the host membranes. Pore-filling was confirmed with SEM analysis. AC impedance spectroscopy was used to measure the conductivity of the membranes.

Following are the conclusions of this study:

1) Polymer-filled nanoporous membranes were fabricated.

2) Conductivities of fabricated composite membranes are a function of thickness. Conductivities of thicker membranes are higher than conductivites of thinner membranes (Figure 3.7).

3) Conductivities of fabricated composite membranes are a function of pore sizes of the host membranes. Conductivities are higher when the pore sizes are smaller (Figure 4.1).

4) Conductivities of fabricated composite membranes are a function of porosity of the host membranes. Conductivities are higher when porosity is more (Figure 4.1).

5) For a polymer to successfully fill the pores of a host membrane, the viscosity and contact angle (of the polymer solution on the host membrane) must be low. The radius of gyration of the polymer must be less than the pore diameter of the host membrane (Section 4.2).

LIST OF REFERENCES

1. Gronowski, A.A. Jiang, M. Yeager, H.L. Wu, G. and Eisenberg, A. Structure and Properties of Hydrocarbon Ionomer Membranes. 1. Poly(methyl methacrylate-co-methacrylic acid). J. Membr. Sci. 1993; 82:83.

2. Grotthuss, C. J. T. de, Sur la décomposition de l'eau et des corps qu'elle tient en dissolution à l'aide de l'électricité galvanique. Ann. Chim. LVIII 1806; 54:74.

3. Zawodzinski, T.A., Jr., Springer, T.E., Davey, J., Jestel, R. and Gottesfeld, S., A Comparative study of water uptake by and transport through Ionomeric fuel cell membranes. J. Electrochem. Soc. 1993; 140:1981.

4. Hsu, W.Y. Barkley, J.R. and Meakin, P. Ion Percolation and Insulator-to-Conductor Transition in Nafion Perfluorosulfonic Acid Membranes. Macromolecules 1980; 13:198.

5. Gierke, T.D. Munn, G.E. and Wilson, F.C. The Morphology in Nafion Perfluorinated Membrane Products, as Determined by Wide- and Small-Angle X-Ray Studies, J. Polym. Sci.: Polym. Phys. Ed. 1981; 19:1687.

6. Carretta, N., Tricoli, V., Comparative investigation of proton and methanol transport in fluorinated ionomeric membranes. J. Electrochem. Soc. 2000; 147:1286.

7. Elabd, Y.A., Napadensky, E., Sloan, J.M. Crawford, D.M. and Walker, C.W. Triblock Copolymer Ionomer Membranes Part I. Methanol and Proton Transport. J. Membr. Sci. 2003; 217: 227.

8. Wang, J.T., Wainright, J.S., Savinell R.F. and Litt, M., A Direct Methanol Fuel Cell Using Acid-Doped Polybenzimidazole as Polymer Electrolyte, J. Appl. Electrochem.1996; 26:751.

9. Scott, W.M., Taama, P., Argyropoulos, Performance of the direct methanol fuel cell with radiation-grafted polymer membranes, J. Membr. Sci. 2000; 171:119.

10. Stangar, U.L., Groselj, N., Orel, B., Schmitz, A. and Colomban, P., Proton-Conducting Sol-Gel Hybrids Containing Heteropoly Acids, Solid State Ionics 2001; 145:109.

11. Libby, B. Smyrl, W. H. and Cussler, E. L., Polymer-Zeolite Composite Membranes for Direct Methanol Fuel Cells, AIChE J. 2003; 91:991.

12. Shahinpoor, M. and Kim. K. J., The effect of surface–electrode resistance on the performance of ionic polymer–metal composites (IPMC) artificial muscles Smart Mater. Struct 2000*;* 9:543.

13. Noh T G, Tak Y, Nam J D, Jeon JW,Kim HM, Choi H R and Bae S,Development of large-surface Nafion–metal composite actuator and its electrochemical characterization Proc. Smart Structures and Materials *2001:* Electroactive

14. Pourcelly, S. ,Applications of Perfluorinated membranes and proton conductors (Nations), in P. Colomban (Ed.), Proton Conductors Solids, Membranes and Gels materials and Devices, Cambridge University Press, 1992, pp. 294-310 and 487-498.

15. Kuwata, S., Miuria, N. and Yamazoe, N., A Solid state amperomeric oxygen sensor using Nation membrane operative at room temperature, Chem. Lett.1988; 1197.

16. Morris, D.R., Sun, X. and Yang L., Development of electrochemical sensors for hydrogen oxygen and water using perfluorosulfonic acid membranes, ACS Syrup. Ser., 480, American Chemical Society, Washington DC, 1992, Chap. 14, pp. 240-253.

17. Sima et al., An electrochemical "Nafion" matrix oxygen sensor and the evaluation of oxygen permeation in coated films. J. Appl. Etectrochem.1993, 23:1102.

18. Weiss, R.A. Sen, A. Pottick, L.A. and Willis, C.L., Block Copolymer Ionomers: 2. Viscoelastic and Mechanical Properties of Sulfonated Poly(styrene-ethylene/butylene-styrene), Polymer 1991; 32:2785.

19. Lu, X., Steckle, W.P., Weiss, R.A., Ionic aggregation in a block copolymer ionomer, Macromolecules 1993; 26:5876.

20. Elabd, Y.A. Walker ,C. W. and Beyer ,F.L. Triblock copolymer ionomer membranes Part II. Structure characterization and its effects on transport properties and direct methanol fuel cell performance. Journal of Membrane Science 2004; 231:181.

21. Cable, K. M. Mauritz, K. A. and Moore, R.B. Anisotropic Ionic Conductivity in Uniaxially 3 Oriented Perfluorosulfonate Ionomers. Chem. Mater. 1995; 7:1601.

22. Oren Y., Freger V., Linder C., Highly conductive ordered heterogeneous ion-exchange membranes, Journal of Membrane Science, 2004; 239:17

23. Martin, C.R., Nanomaterials-A Materials based Synthetic Approach, Science 1994; 266:1961.

24. Mansouri, J. Burford, R.P., Novel Membranes from Conducting Polymers, J. Membr. Sci. 1994; 87:23.

25. Granstrom, M. Inganas, O. Electrically Conductive Polymer Fibers with Mesoscopic Diameters. 1. Studies of Structure and Electrical Propertiesties. Polymer 1995; 36:2867.

26. Pra, L. D.-D. Ferain, E. Legras, R. Demoustier-Champagne, S. Fabrication of a New Generation of Track-Etched Templates and Their Use for Synthesis Metallic and Organic Nanostructures, Nuclear Instruments and Methods in Physics Research B 2002; 196: 81.

27. Fang, Y. and Leddy, J. Surface Diffusion in Microstructured, Ion-Exchange Matrices: Nafion/Neutron Track-Etched Polycarbonate Membrane Composites. J. Phys. Chem. 1995; 99:6064.

28. Vorrey, S. and Teeters, D., Study of the Ion Conduction of Polymer Electrolytes Confined in Micro and Nanopores, Electrochimica Acta 2003; 48:2137.

29. Yamaguchi, T. Nakao, S. and Kimura, S., Swelling Behavior of the Filling-Type Membrane, J. Polym. Sci. Part B. Polym. Phys. 1997; 35:469.

30. Yamaguchi, T. Miyata, F. Nakao, S., Polymer Electrolyte Membrane with a Pore-Filled Structure for a Direct Methanol Fuel Cell, Adv. Mater. 2003; 15:1198.

31. Smela, E., Conjugated polymer actuators for biomedical applications, Adv. Mat. 2003; 6:15.

32. Elabd, Y. A., Napadensky, E., Sulfonation and characterization of poly(styrene-isobutylene-styrene) triblock copolymers at high ion-exchange capacities, Polymer 2004; 45: 3037.

33. Sperling, L. H., Introduction to Physical Polymer Science, Third edition, Wiley Interscience 2001; 5:174.

34. Galeska, I., Chattopadhyay, D., Moussy, F., Papadimitrakopoulos, F., Calcification-resistant Nafion/Fe3+ assemblies for implantable biosensors, Biomacromolecules 2000; 1:202.

APPENDIX A: VISCOSITY MEASUREMENT

Table A1 Viscosity data for SPS/acetone.

S. No.	Speed (RPM)	Number	Reading	Viscosity (cP)
1	0.5	8000	0	0
2	1	4000	0	0
3	2.5	1600	0	0
4	5	800	0	0
5	10	400	0	0
6	20	200	0.05	10
7	50	80	0.05	4
8	100	40	0.1	4

Table A2 Viscosity data for SPS/DMSO

S. No.	Speed (RPM)	Number	Reading	Viscosity (cP)
1	0.5	8000	0	0
2	1	4000	0.05	200
3	2.5	1600	0.05	80
4	5	800	0.05	40
5	10	400	0.1	40
6	20	200	0.1	20
7	50	80	0.25	20
8	100	40	0.45	18

Table A3 Viscosity data for Nafion® (Ion Power)

S. No.	speed (RPM)	Number	Reading	Viscosity (cP)
1	0.5	8000	0	0
2	1	4000	0	0
3	2.5	1600	0	0
4	5	800	0.05	40
5	10	400	0.05	20
6	20	200	0.05	10
7	50	80	0.1	8
8	100	40	0.2	8

Table A4 Viscosity data for Nafion® (Aldrich)

S. No.	Speed (RPM)	Number	Reading	Viscosity (cP)
1	0.5	8000	0	0
2	1	4000	0	0
3	2.5	1600	0	0
4	5	800	0.05	40
5	10	400	0.1	40
6	20	200	0.1	20
7	50	80	0.2	16
8	100	40	0.4	16

Table A5 Summary of viscosities for solutions.

S. No.	Solution	Viscosity (cP)
1	SPS/Acetone	4
2	SPS/DMSO	19
3	Nafion® (Ion Power)	8
4	Nafion® (Aldrich)	16

The viscosity calculations for a particular speed of rotation of the spindle were made by multiplying the number by the digital reading. The averages of steady state viscosity values were taken. These usually occurred at the highest two spinning speeds. Ta low speeds the digital reading is usually zero. For the SPS/Acetone solution, the average viscosity was measured to be 4 cP. For the SPS/DMSO solution, the average viscosity was measured to be 19 cP. For the Nafion® (Ion Power) solution, the average viscosity was measured to be 8 cP. For the Nafion® (Aldrich) solution, the average viscosity was measured to be 16 cP.

APPENDIX B: CONTACT ANGLE MEASUREMENT

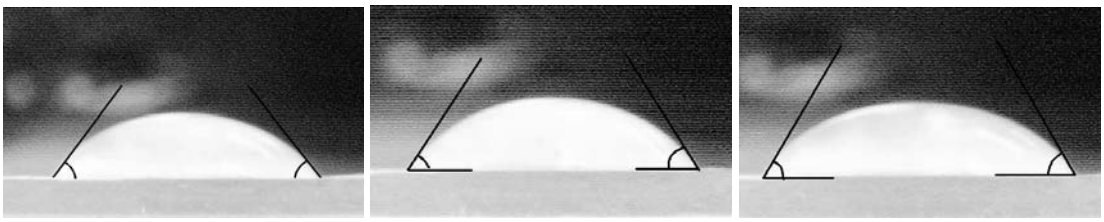

Figure B1 Contact angles for water-PCTE.

From Figure B1 (a), (b), and (c) it can be seen that the contact angles for water PCTE are 52^{o}, 55^{o} and 58^{o} for three different experiments. This is equivalent to an average value of 55^{o}.

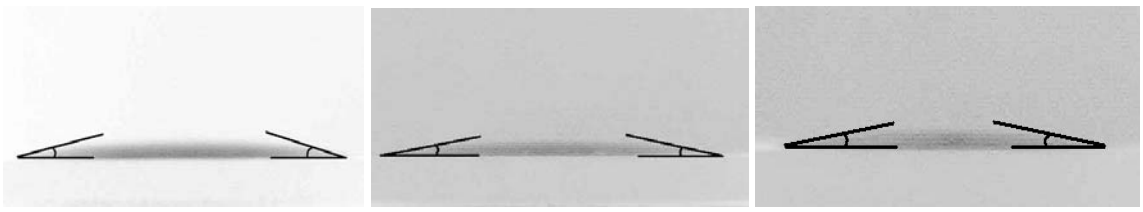

(a) (b) (c)

Figure B2 Contact angles for SPS/DMSO-PCTE.

From Figure B2 (a), (b), and (c) it can be seen that the contact angles for SPS/DMSO are 13^{o}, 9^{o} and 9^{o} for three different experiments. This is equivalent to an average value of 10.33^{o}.

(a) (b) (c)

Figure B3 Contact angles for SPS/Acetone-PCTE.

From Figure B3 (a), (b), and (c) it can be seen that the contact angles for SPS/Acetone are close to zero for three different experiments. On coming into contact with the PCTE, the SPS/Acetone spreads out.

From Figure B4: (a), (b), (c) and (d) it can be seen that the contact angles for Nafion® (Aldrich) are 31^{o}, 23^{o}, 22^{o} and 23.5^{o} for four different experiments. This is equivalent to an average value of 24.875^{o}.

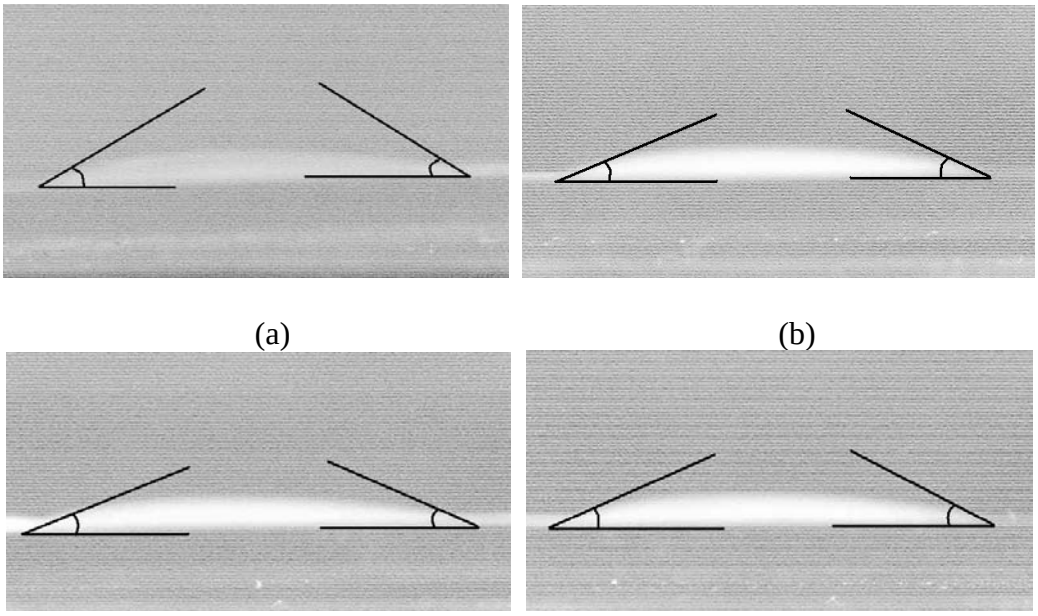

(a) (b)

(c) (d)

Figure B4 Contact angles for Nafion® Aldrich-PCTE.

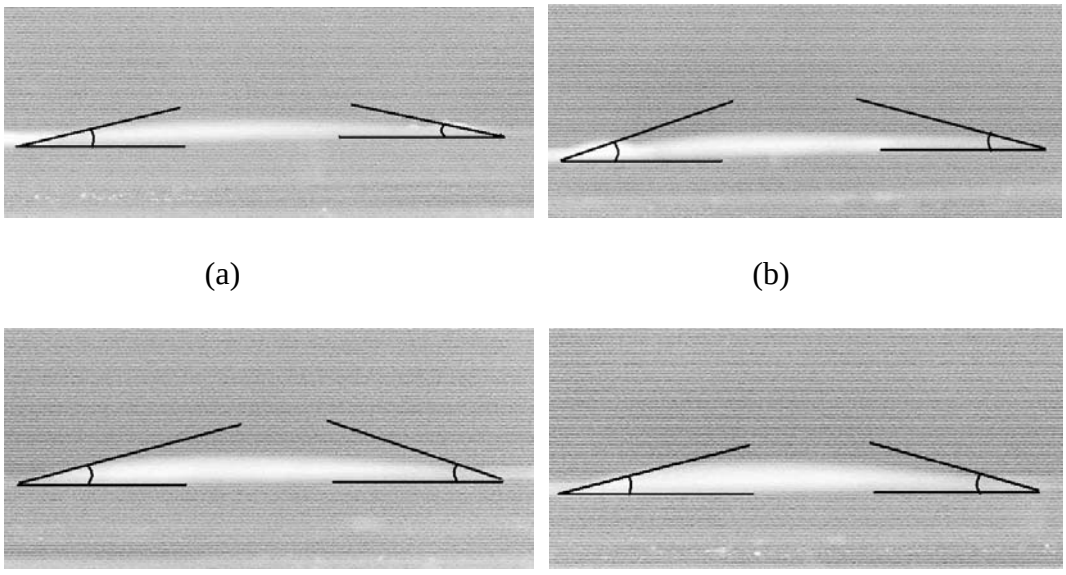

(a) (b)

(c) (d)

Figure B5 Contact angles for Nafion® Ion Power-PCTE.

From Figure B5 (a), (b), (c) and (d) it can be seen that the contact angles for Nafion® (Ion Power) are 12.5^{o}, 15.5^{o}, 16.5^{o} and 15^{o} for three different experiments. This is equivalent to an average value of 14.875^{o}. The following table summarized the results for contact angle measurements for different solutions on PCTE.

Table B1 Contact angles on PCTE.

S. No.	Solution	Average Contact Angle	Solution Type
1	Water	55^{o}	Wetting
2	SPS/DMSO	10.33^{o}	Wetting
3	SPS/Acetone	0^{o}	Penetrating
4	Nafion® (Aldrich)	24.875^{o}	Wetting
5	Nafion® (Ion Power)	14.875^{o}	Wetting

From Table B1, it is apparent that the only solution that can be classified as penetrating to the surface of PCTE is SPS/Acetone. All other solutions can be classified as wetting.

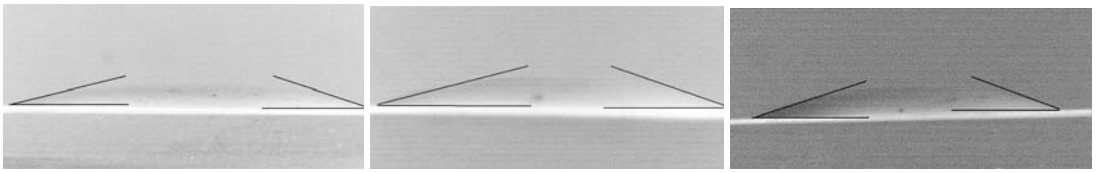

(a) (b) (c)

Figure B6 Contact angles for SPS/DMSO-Alumina.

From Figure B6 (a), (b), and (c) it can be seen that the contact angles for SPS/DMSO are 16.5^{o}, 16^{o} and 19.5^{o} for three different experiments. This is equivalent to an average value of 17.33^{o}.

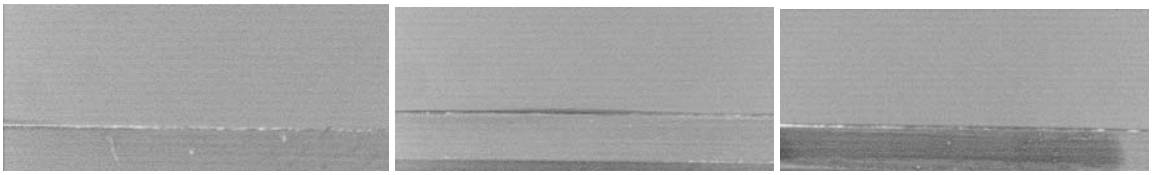

(a) (b) (c)

Figure B7 Contact angles for SPS/Acetone-Alumina.

From Figure B7 (a), (b), and (c) it can be seen that the contact angles for SPS/Acetone are close to zero for three different experiments. On coming into contact with the Alumina, the SPS/Acetone spreads out.

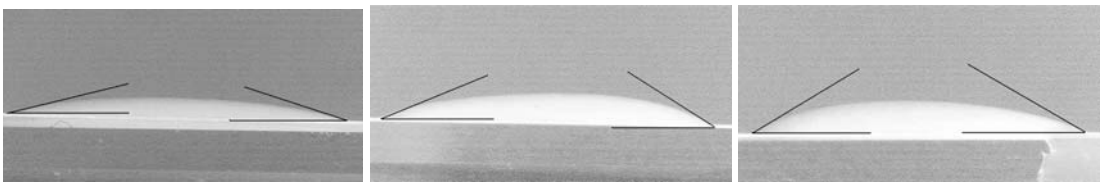

(a) (b) (c)

Figure B8 Contact angles for Nafion® (Aldrich)-Alumina.

From Figure B8 (a), (b), (c) and (d) it can be seen that the contact angles for Nafion® (Aldrich) are 16.5^{o}, 27^{o}and 30^{o} for three different experiments. This is equivalent to an average value of 24.5^{o}.

From Figure B9 (a), (b), (c) and (d) it can be seen that the contact angles for Nafion® (Ion Power) are 18^{o}, 15^{o}and 15^{o}for three different experiments. This is equivalent to an average value of 16^{o}. The following table summarized the results for contact angle measurements for different solutions on PCTE.

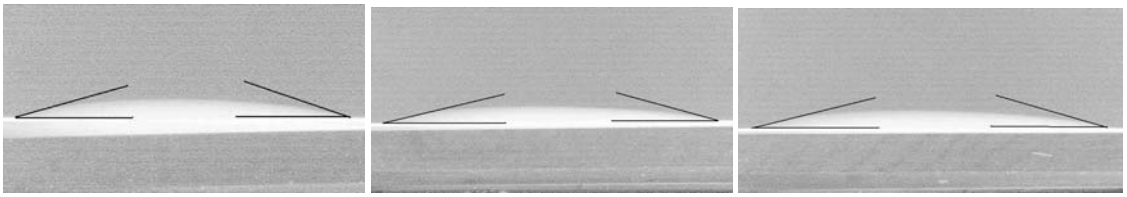

(a) (b) (c)

Figure B9 Contact angles for Nafion® (Ion Power)-Alumina.

Table B2 Contact angles on alumina.

S. No.	Solution	Average Contact Angle	Solution Type
1	SPS/DMSO	17.33^{o}	Wetting
2	SPS/Acetone	0^{o}	Penetrating
3	Nafion® (Aldrich)	24.5^{o}	Wetting
4	Nafion® (Ion Power)	16^{o}	Wetting

APPENDIX C: CONDUCTIVITY DATA

Table C1 conductivity data for sorbed membranes

Membrane number	Conductivity (S/cm)
1	0.00083842
2	0.0030700
3	0.0015840
4	0.0048114
5	0.0043963
6	0.0031578
7	0.0027084
8	0.0034092
9	0.0031116
10	0.0021676
11	0.0019209
12	0.0033704
13	0.0039234
14	0.0021200
15	0.0029287

Table C2 conductivity versus thickness for sorbed PCTE membranes

L_t/L_b	Conductivity (S/cm)
15.667	0.017100
18.167	0.017100
11.500	0.016900
10.000	0.0051660
8.1667	0.0023290
10.667	0.0038070
10.333	0.0051400
6.0000	0.0020310
8.3333	0.0023800
8.3333	0.0027800
6.8333	0.0018050
11.500	0.0055500
8.0000	0.0025500
5.6667	0.0023340
7.8333	0.0073740

Table C3 thickness and spincoater speed data for spuncoat membranes

Speed (RPM)	L_t/L_b
1.5000	0.00037185
2.6667	0.0012979
3.5000	0.0024708
3.1667	0.0022916
1.8333	0.0014283
1.3333	0.0011618
3.6667	0.0024585
0.66667	0.00040072
0.66667	0.00029606
1.6667	0.00070937
1.3333	0.00058833
0.83333	0.00034327
2.1667	0.00090183
1.1667	0.00065707
1.5000	0.00037185

Table C4 conductivity and L_t/L_b data for spuncoat membranes

L_t/L_b	Conductivity (S/cm)
15.667	0.017100
18.167	0.017100
11.500	0.016900
10.000	0.0051660
8.1667	0.0023290
10.667	0.0038070
10.333	0.0051400
6.0000	0.0020310
8.3333	0.0023800
8.3333	0.0027800
6.8333	0.0018050
11.500	0.0055500
8.0000	0.0025500
5.6667	0.0023340
7.8333	0.0073740

Table C5 thickness and contact time with DMSO data for spuncoat membranes

L_t/L_b	Contact Time (min)
10.458	1.0000
5.5833	3.0000
3.2000	5.0000
3.3666	8.0000
1.6250	12.000
1.2083	15.000
0.41666	30.000
0.0000	60.000

Table C6 conductivity and L_t/L_b data for filtered and spuncoat SPS/PCTE membranes

L_t/L_b	Conductivity (S/cm)
1.3333	2.1542e-5
1.3333	2.3849e-5
1.3333	1.6228e-5
1.5000	3.1279e-5
1.5000	2.5853e-5
1.6667	3.5951e-5
1.8333	3.9799e-5
2.0000	4.4538e-5

Table C7 conductivities of filtered and spuncoat and filtered and blotted SPS/PCTE membranes (100 nm pore size)

Filtered and spuncoat SPS/PCTE (100 nm pores)		Filtered and blotted SPS/PCTE (100 nm pores)	
L_t/L_b	Conductivity (S/cm)	L_t/L_b	Conductivity (S/cm)
1.3333	2.1542e-5	0.83333	0.00022193
1.3333	2.3849e-5	3.1667	0.0013965
1.3333	1.6228e-5	1.8333	0.00086019
1.5000	3.1279e-5	1.5000	0.00052694
1.5000	2.5853e-5	0.66667	0.00015290
1.6667	3.5951e-5	2.1667	0.00098066
1.8333	3.9799e-5	1.6667	0.00063452
2.0000	4.4538e-5	2.3333	0.0010777

Table C8 conductivity and L_t/L_b data for SPS-PCTE (50 nm pore size) composites

L_t/L_b	Conductivity (S/cm)
0.83333	0.0013438
0.66667	0.0011260
0.0000	0.00054095
2.3333	0.0047550
2.1667	0.0046537
1.5000	0.0028281
1.3333	0.0021045
1.1667	0.0018339

Table C9 conductivity and L_t/L_b data for SPS/alumina (100 nm pore size) composite membranes

L_t/L_b	Conductivity (S/cm)
0.55172	0.0079318
0.51724	0.0031562
0.43103	0.0025773
0.37931	0.0019832
0.24138	0.0013430
0.29310	0.0017761

Table C10 conductivity and L_t/L_b data for SPS/alumina composites (20 nm pore size)

L_t/L_b	Conductivity (S/cm)
0.034483	0.0049428
0.068966	0.0059636
0.17241	0.012200
0.034483	0.0050948
0.68966	0.029796
0.034483	0.0053509